International
Progress Report

IPR-99-11

Äspö Hard Rock Laboratory

Preparatory modelling for the backfill and plug test

Scoping calculations of H-M processes

Lennart Börgesson
Clay Technology AB

Jan Hernelind
FEMTech AB

July 1998

Svensk Kärnbränslehantering AB
Swedish Nuclear Fuel
and Waste Management Co
Box 5864
SE-102 40 Stockholm Sweden
Tel +46 8 459 84 00
Fax +46 8 661 57 19

Äspö Hard Rock
Laboratory

Report no.	No.
IPR-99-11	F61K
Author	Date
Lennart Börgesson, Jan Hernelind	July 1998
Checked by	Date
Christer Svemar	1999- 06-01
Approved	Date
Olle Olsson	1999-06-04

Äspö Hard Rock Laboratory

Preparatory modelling for the backfill and plug test

Scoping calculations of H-M processes

Lennart Börgesson
Clay Technology AB

Jan Hernelind
FEMTech AB

July 1998

Keywords: Backfill, plug rock, modelling, hydraulic, mechanical, finite element

Abstract

This document is a report on the results from preparatory modelling of hydro-mechanical processes in the Backfill and Plug Test in Äspö HRL. The work has consisted of determining parameters and calibrating material models with laboratory results as well as simulation of especially the hydraulic processes in the experiment. The following simulations, made with the finite element program ABAQUS, are described:

- The water saturation process in the backfill
- Water flow and water pressure in the backfill and near-field rock during the flow test sequence
- Water flow and water pressure in the rock near the tunnels surrounding the test site

Sammanfattning

Denna rapport redovisar resultat från förberedande modellering av hydro-mekaniska processer i återfyllnings- och pluggningsförsöket (Backfill and Plug Test) i Äspö HRL. Arbetet har bestått i att dels bestämma parametrar och kalibrera materialmodeller med hjälp av laboratorieresultat ,dels simulera främst de hydrauliska processerna under försökets gång. Följande simuleringar, som gjorts med finita elementprogrammet ABAQUS, redovisas:

- Vattenmättnadsprocessen i återfyllningen
- Vattenflöde och vattentryck i återfyllning och närfältsberg under flödestesterna
- Vattenflöde och vattentryck i berget runt de tunnlar som ligger i närheten av försöksplatsen

Executive Summary

This document is a report on the results from preparatory modelling of hydro-mechanical processes in the Backfill and Plug Test in Äspö HRL. The work has consisted in determining parameters and calibrating material models with laboratory results as well as simulation of especially the hydraulic processes in the experiment. The following simulations, made with the finite element program ABAQUS, are described:

- The water saturation process in the backfill
- Water flow and water pressure in the backfill and near-field rock during the flow test sequence
- Water flow and water pressure in the rock near the tunnels surrounding the test site

These calibrations and scoping calculations show for example the following:

The influence of the degree of saturation S_r of the backfill on the hydraulic conductivity is very strong (S_r^{10}).

A water pressure of about 500 kPa is required in the filter mats in order to reach complete saturation in the backfill containing 30% bentonite within one year.

A sensitivity analysis of the flow testing after water saturation indicates that the hydraulic conductivity of the naturally fractured zones and the undisturbed rock has an insignificant influence on the measured results. It also indicates that it will be difficult to distinguish between the water flow in the disturbed zone and the backfill if the hydraulic conductivity of the disturbed zone is on the same order of magnitude or lower than the hydraulic conductivity of the backfill

The hydraulic model of the rock around the test tunnel and the near by tunnels can have boundaries with constant hydrostatic pressure. The model should include a skin zone around the tunnels, and the major naturally fractured zones intersecting the test tunnel.

Contents

1 Introduction

The Äspö Hard Rock Laboratory is constructed with the aim of providing possibilities for research, development and demonstration in a realistic and undisturbed underground environment at the depth which is considered for the deep repository. The Backfill and Plug Test is one project that will be performed in Äspö HRL with the purposes to

- develop and test different materials and compaction techniques for backfilling of tunnels excavated by blasting
- test the function of the backfill and its interaction with the surrounding rock in full scale in a tunnel excavated by blasting
- develop technique for building tunnel plugs and test the function

An important part of the work is to understand the thermal, hydraulic, and mechanical processes in the backfill and near field rock during the test and to be able to model these processes so that predictions of the behaviour of the backfill in a deep repository can be made.

The modelling work can be divided into the following steps:

1. Laboratory testing of backfill properties
2. Determination and calibration of material models
3. Scoping calculations of the processes for the purposes of design and general understanding
4. Predictions without knowledge of any field results
5. Evaluation of the models and measured results and improvement of the models

This report deals with steps 2 and 3. The laboratory tests will be running during all steps.

2 Backfill and Plug Test

The Backfill and Plug Test is described in the test plan /2-1/. The test is located in the old ZEDEX tunnel as shown in Fig 2-1. The test will be made in the old part of the tunnel that was excavated by normal blasting. The extension, that has been excavated with very careful blasting, will not be used for the test. Fig 2-2 shows an overview of the test. The test region can be divided into the following three test parts:

1. The *inner part* filled with backfill containing 30 % bentonite.

2. The *outer part* filled with backfill without bentonite.

3. The *plug*.

The inner test part will be filled with a mixture of 30 % bentonite and crushed granite rock. The outer test part of the tunnel will be filled with crushed rock without addition of bentonite, except for the upper 10-20 cm, where a slot will be left and filled with blocks of highly compacted bentonite/crushed rock mixture and bentonite pellets. The backfill will be compacted with inclined compaction, a technique developed in preparatory field tests. Both the inner and outer part will be divided into five sections parted by drainage layers of permeable mats. Outside the backfill an approximately 3 meter thick plug will be placed with the required function of both being a mechanical support and a hydraulic seal.

The backfill and rock will be instrumented with piezometers, total pressure cells, thermocouples, moisture gauges, and gauges for measuring the local hydraulic conductivity. The axial conductivity of the backfill and the near field rock will after water saturation be tested by applying a water pressure gradient along the tunnel between the mats and measuring the water flow. The flow close to the floor and roof respectively as well as in the central part of the backfill will be measured separately. The hydraulic function of the plug will be tested in a similar way. The mechanical interaction between a simulated swelling buffer material and the backfill and between the roof and the backfill will be tested with pressure cylinders fixed to the floor and the roof of the tunnel.

3 Finite element code

3.1 General

The finite element code ABAQUS was used for the calculations. ABAQUS is originally designed for non-linear stress analyses. It has been extended very much in the last 5-10 years and contains today a capability of modelling a large range of processes in many different materials as well as complicated three-dimensional geometry.

Detailed results from ABAQUS may be obtained via a post-processing code ABAQUS/Post. The code includes special material models for rock and soil and ability to model geological formations with infinite boundaries and in situ stresses by e.g. the own weight of the medium.Detailed information of the available models, application of the code and the theoretical background is given in the ABAQUS Manuals /3-1/.

3.2 Hydro-mechanical analyses in ABAQUS

The hydromechanical model consists of porous medium and wetting fluid and is based on equilibrium, constitutive equations, energy balance and mass conservation using the effective stress.

Equilibrium

Equilibrium is expressed by writing the principle of virtual work for the volume V (enclosed by the surface S) under consideration in its current configuration at time t:

$$\int_V \boldsymbol{\sigma} : \delta\boldsymbol{\varepsilon}\, dV = \int_S \mathbf{t} \cdot \delta\mathbf{v}\, dS + \int_V \hat{\mathbf{f}} \cdot \delta\mathbf{v}\, dV, \qquad \textbf{(3-}1\textbf{)}$$

where $\delta\mathbf{v}$ is a virtual velocity field, $\delta\boldsymbol{\varepsilon} \overset{def}{=} sym\left(\partial\delta\mathbf{v}/\partial\mathbf{x}\right)$ is the virtual rate of deformation, $\boldsymbol{\sigma}$ is the true (Cauchy) stress, $\mathbf{t}$ are the surface tractions per unit area, and $\hat{\mathbf{f}}$ are body forces per unit volume. For our system, $\hat{\mathbf{f}}$ will often include the weight of the wetting liquid,

$$\mathbf{f}_w = S_r n \rho_w \mathbf{g}, \qquad (3\text{-}2)$$

where S_r is the degree of saturation, n the porosity, ρ_w the density of the wetting liquid and $\mathbf{g}$ is the gravitational acceleration, which we assume to be constant and in a constant direction (so that, for example, the formulation cannot be applied directly to a centrifuge

experiment unless the model in the machine is small enough that g can be treated as constant). For simplicity we consider this loading explicitly so that any other gravitational term in $\hat{\mathbf{f}}$ is only associated with the weight of the dry porous medium. Thus, we write the virtual work equation as

$$\int_V \boldsymbol{\sigma} : \delta\boldsymbol{\varepsilon} dV = \int_s \mathbf{t} \cdot \delta\mathbf{v} dS + \int_V \mathbf{f} \cdot \delta\mathbf{v} dV + \int_V S_r n \rho_w \mathbf{g} \cdot \delta\mathbf{v} dV, \tag{3-3}$$

where **f** are all body forces except the weight of the wetting liquid.

The simplified equation used in ABAQUS for the effective stress is:

$$\overline{\boldsymbol{\sigma}}^* = \boldsymbol{\sigma} + \chi u_w \mathbf{I}. \tag{3-4}$$

where $\boldsymbol{\sigma}$ is the total stress, u_w is the porewater pressure, χ is a function of the degree of saturation (usual assumption $\chi = S_r$), and **I** the unitary matrix.

Energy balance

The conservation of energy implied by the first law of thermodynamics states that the time rate of change of kinetic energy and internal energy for a fixed body of material is equal to the sum of the rate of work done by the surface and body forces. This can be expressed as:

$$\frac{d}{dt}\int_V \left(\tfrac{1}{2}\rho \mathbf{v} \cdot \mathbf{v} + \rho U\right) dV = \int_s \mathbf{v} \cdot \mathbf{t} dS + \int_V \mathbf{f} \cdot \mathbf{v} dV, \tag{3-5}$$

where

ρ is the current density,

v is the velocity field vector,

U is the internal energy per unit mass,

t is the surface traction vector and

f is the body force vector.

Constitutive equations

The constitutive equation for the solid is expressed as:

$$d\boldsymbol{\tau}^{c} = \mathbf{H} : d\boldsymbol{\varepsilon} + \mathbf{g}, \tag{3-6}$$

where $d\boldsymbol{\tau}^{c}$ is the stress increment, $\mathbf{H}$ the material stiffness, $d\boldsymbol{\varepsilon}$ the strain increment and $\mathbf{g}$ is any strain independent contribution, defined in terms of the current state, direction for straining, etc., and of the kinematic assumptions used to form the generalized strains.

The constitutive equation for the liquid (static) in the porous medium is expressed as:

$$\frac{\rho_w}{\rho_w^0} \approx 1 + \frac{u_w}{K_w} - \varepsilon_w^{th}, \tag{3-7}$$

where ρ_w is the density of the liquid, ρ_w^0 is its density in the reference configuration, u_w is the pore water pressure, $K_w(T)$ is the liquid's bulk modulus, and

$$\varepsilon_w^{th} = 3\alpha_w (T - T_w^0) - 3\alpha_{w|T^I} (T^I - T_w^0) \tag{3-8}$$

is the volumetric expansion of the liquid caused by temperature change. Here $\alpha_w(T)$ is the liquid's thermal expasion coefficient, T is the current temperature, T^I is the initial temperature at this point in the medium, and T_w^0 is the reference temperature for the thermal expansion. Both u_w / K_w and ε_w^{th} are assumed to be small.

Mass conservation

The mass continuity equation for the fluid combined with the divergence theorem implies the pointwise equation:

$$\frac{1}{J}\frac{d}{dt}\left(J\rho_w S_r n\right) + \frac{\partial}{\partial \mathbf{x}} \cdot \left(\rho_w S_r n \mathbf{v}_w\right) = 0. \tag{3-9}$$

where J is the determinant of the Jacobian matrix and $\mathbf{x}$ is position. The constitutive behavior for pore fluid is governed by Darcy's law, which is generally applicable to low fluid velocities. Darcy's law states that, under uniform conditions, the volumetric flow rate of the wetting liquid through a unit area of the medium, $S_r n \mathbf{v}_w$, is proportional to the negative of the gradient of the piezometric head:

$$S_r n \mathbf{v}_w = -\hat{\mathbf{k}} \frac{\partial \phi}{\partial \mathbf{x}}, \tag{3-10}$$

where $\hat{\mathbf{k}}$ is the permeability of the medium and ϕ is the piezometric head, defined as:

$$\phi \overset{\text{def}}{=} z + \frac{u_w}{g\rho_w}, \tag{3-11}$$

where z is the elevation above some datum and g is the magnitude of the gravitational acceleration, which acts in the direction opposite to z. $\hat{\mathbf{k}}$ can be anisotropic and is a function of the saturation and void ratio of the material. $\hat{\mathbf{k}}$ has units of velocity (length/time). [Some authors refer to $\hat{\mathbf{k}}$ as the hydraulic conductivity and define the permeability as

$$\hat{\mathbf{K}} = \frac{\nu}{g}\hat{\mathbf{k}}, \tag{3-12}$$

where ν is the kinematic viscosity of the fluid.]

We assume that g is constant in magnitude and direction, so

$$\frac{\partial \phi}{\partial \mathbf{x}} = \frac{1}{\mathrm{g}\rho_{\mathrm{w}}}\left(\frac{\partial \mathrm{u}_{\mathrm{w}}}{\partial \mathbf{x}} - \rho_w \mathbf{g}\right), \tag{3-13}$$

4 Material models for the backfill and the rock

4.1 General

Only hydro-mechanical models have been used since no change in temperature is imposed on the backfill in the test.

4.2 Material models for the backfill

4.2.1 Hydraulic

Unsaturated flow in ABAQUS is modelled with Darcy's law in a porous material and by using the negative pore water pressure in the unsaturated material as driving force. The magnitude of the hydraulic conductivity K_p of partly saturated clay is a function of the void ratio, the degree of saturation and the temperature. K_p is expressed as a function of the hydraulic conductivity K of saturated clay according to Eqn 4-1.

$$\boldsymbol{K_p} = \left(\boldsymbol{S_r}\right)^{\delta} \boldsymbol{K} \tag{4-1}$$

where

K_p = hydraulic conductivity of partly saturated soil (m/s)

K = hydraulic conductivity of completely saturated soil (m/s)

S_r = degree of water saturation

δ = parameter (usually between 3 and 10)

The "standard" value of δ is 3, which is used for highly compacted bentonite with no ballast material.

Required input data for the unsaturated flow calculations are

- The saturated hydraulic conductivity K, which can be made a function of the void ratio e and the temperature T.
- The parameter δ in the expression for the unsaturated hydraulic conductivity

- The pore pressure of the backfill material u as a function of the degree of saturation S_r.

4.2.2 Mechanical

Effective stress concept

The backfill is mechanically modelled as a porous material with simple linear elasticity with the parameters Young's modulus E and Poisson's ratio v.

The effective stress concept according to Bishop is used for modelling the mechanical behaviour of the water-unsaturated backfill material (Eqn 4-2).

$$s_e = (s - u_a) + \chi(u_a - u_w) \tag{4-2}$$

where

χ = a parameter related to the degree of saturation.

s_e = effective stress

s = total stress

u_a = pore gas pressure

u_w = pore water pressure

Eqn 4-2 has been simplified in the following way:

u_a = 0 (no account is taken to pressure of enclosed air)

$\chi = S_r$

Moisture swelling

The shortcomings of the effective stress theory can be partly compensated in ABAQUS by a correction called "moisture swelling". This procedure changes the volumetric strain ε_v by adding a strain that can be made a function of the degree of saturation S_r according to Eqn 4-3.

$$\Delta\varepsilon_v = f(S_r) \tag{4-3}$$

Properties of the separate phases

The water and the particles are mechanically modelled as separate phases with linearly elastic behaviour. The following values were used for all calculations:

$B_s = 2.1 \cdot 10^8$ kPa (Bulk modulus of the solid grains)

$B_w = 2.1 \cdot 10^6$ kPa (Bulk modulus of water)

4.3 Material models for the rock

4.3.1 Hydraulic

Water flow is modelled with Darcy's law in a porous material with a constant hydraulic conductivity. Unsaturated conditions of the rock has not been modelled.

4.3.2 Mechanical

The rock has been modelled as a linearly elastic porous material with Young's modulus E and Poisson's ratio ν.

5 Calibration of the hydraulic model of unsaturated backfill

5.1 General

Before flow testing of the backfill and near-field rock can start the backfill must be water saturated. Laboratory measurements have shown that the rate of water uptake and water saturation of the bentonite mixed backfill is slow and will thus be critical for when the flow testing can start. An estimation of the time until saturation has been done. It has been preceded by determination of relevant material parameters.

5.2 Parameter values for the material model

5.2.1 Backfill materials

30% bentonite and 70% crushed rock of the type that will be used in the test has been tested in the laboratory with respect to the hydraulic behaviour /5-1/. The basic material models have been made for the following ”reference material” which assumes that the average degree of compaction achieved in the field will be 90% modified Proctor. According to compaction tests 90% Proctor corresponds to the following initial properties (index 0 refer to the initial state of variables or parameters that are not constants):

ρ_{d0}=1.75 t/m^3 (dry density)

e_0=0.57 (void ratio)

w_{m0}=20.7 % (water ratio at saturation)

5.2.2 Uncalibrated material model

The measurements of hydraulic conductivity have yielded the following average value at the reference density (saturated and percolated with Äspö water, which contains 1.2 % salt):

K=2.0x10^{-10} m/s

The relation between suction s_w and water ratio of the backfill material has been measured and transformed to degree of saturation. The following relation has been used for the reference material:

S_r	s_w kPa
0.01	400 000
0.28	50 000
0.33	20 000
0.40	12 000
0.43	5 000
0.48	3 000
0.58	1 050
0.67	500
0.77	230
0.87	110
0.92	80
0.97	50
0.995	40
1.0	0

Fig 5-1 shows the measured values of matric suction as a function of water ratio and the relation used in the calculations. Measured results of total suction are also shown in the figure. The difference between total and matric suction is the osmotic suction. Osmotic suction is assumed not to be included as a driving force for the water transport.

Before calibration the same value of the parameter δ (Eqn 4-1) of the unsaturated hydraulic conductivity was used as for buffer material:

$\delta = 3$

5.2.3 Simulation of laboratory tests of the water uptake process

A number of tests of unsaturated water flow have been performed in the laboratory /5-1/. Water was applied at one end of confined samples and the water ratio distribution measured by cutting the samples in thin slices at different times. Backfill material with the following two different initial water ratios were used in the tests.

Material A: w_o=6.3 % which yields the following initial conditions in the backfill:

e_0=0.57

S_{r0}=0.33

u_0=-20 000 kPa

Material B: w_0=12.0 % which yields the following initial conditions in the backfill:

e_0=0.57

S_{r0}=0.58

u_0=-1 050 kPa

In order to simulate the in situ conditions Äspö water was used during both mixing and testing.

The calculated and measured water ratios at different times are shown in Fig 5-2. The comparison shows that the agreement is poor. The following two main deviations can be noted:

- The calculated water uptake is too fast
- The shape of the curves disagree

5.2.4 Calibrated material models

In order to get a better agreement the parameters d and K for the unsaturated hydraulic conductivity were calibrated, which yielded the following revised values:

Material A:

δ= 10

Material B:

δ= 10

K=0.5x10^{-10} m/s

For material A, which had a low initial water ratio, a change in δ was sufficient to reach a good agreement between measured and calculated results, while for material B, which had a high initial water ratio, the basic hydraulic conductivity needed to be slightly changed as well.

5.2.5 Results of the final simulations of the laboratory tests

The laboratory tests were made with 10 cm high samples. The finite element model of the sample was made with 21 elements which were mechanically fixed and hydraulically confined, the latter with the exception of the bottom boundary which was set with a fixed pore pressure of

u = 0 kPa.

The element mesh and the change in water ratio with time are shown in Fig 5-3 for the two calculations with the calibrated material models.

Fig 5-4 shows a comparison of the measured and calculated results. The agreement is very good for these material models.

5.3 Conclusions

Calibration of the parameter δ in the relation for the unsaturated hydraulic conductivity yielded a material model that very well simulated the laboratory tests. However, the model of the backfill with a high initial water ratio required a change in K to a value that is 4 times lower than the other model. The reason why different K values are required is not completely understood, but experiences of measured hydraulic conductivity show that the initial water ratio at compaction has an influence on the hydraulic conductivity and that a high initial water ratio usually yields a lower hydraulic conductivity than a low initial water ratio.

6 Calculation of the water saturation process in a backfill section

6.1 Element mesh

The saturation of the backfill sections in the test will be made artificially from one filter layer while the filter on the other side of the backfill section will be used for deairing. One section is 2.2 m thick 4.5 m high and is inclined 35-45 degrees. It has been modelled with a 2D element mesh, that is shown in Fig 6-1. 25 m of rock in both the floor and the roof has been included as well as 0.3 m disturbed zone in the roof and 0.8 m disturbed zone in the floor of the rock. The rock outside the disturbed zone is not active in this calculation. The filters have been taken into account with a 2.5 cm thick element layer on both sides of the backfill section.

6.2 Material models

Backfill

The revised calibrated material models shown in chapter 5 have been used for the calculations. Two calculations with the initial conditions for materials A and B have been done which means that backfill compacted to 90% modified Proctor with the water ratios 6.3 % and 12.0 % has been simulated.

Rock

The rock has been hydraulically modelled as a porous medium with the following properties:

Undisturbed rock:

K=1.0x10^{-10} m/s

e=0.0001

Disturbed zone:

K=1.0x10^{-9} m/s

e=0.0005

u_0=0 is applied as initial condition for the pore pressure in all nodes in the rock. All nodes have been mechanically constrained in this calculation.

6.3 Boundary conditions

The hydraulic boundary conditions are the following:

- u=0 in the outer boundary of the undisturbed rock and in the filter on the right side of the backfill section
- isolated (no flow) conditions on the other boundaries

The model is 2-dimensional which means that no account has been taken to the water coming from the rock walls. On the other hand the high hydraulic conductivity of the disturbed zone yields that water is freely available in the roof and floor, which probably overestimates the water supply from those parts. Since the water pressure in the filter is artificial this boundary condition is correct and dominates the water uptake process.

All boundaries have been mechanically constrained.

6.4 Results

The calculations have been run to cover a period of 12.7 years ($4 \cdot 10^8$ seconds) and the results plotted at 4 times.

Material A (w_o=6.3 %)

The results are shown in Figs 6-2 as a contour plot and history plots. The backfill is completely saturated after less than 1.6 years.

Material B (w_o=12.0 %)

The results are shown in Figs 6-3 and 6-4 as contour plots and history plots. The backfill is completely saturated after 12.7 years and more than 90 % saturated after 6.3 years.

6.5 Calculations with high water pressure in the filter mats

The preliminary choice is to use a high initial water ratio of the 30/70 backfill material, (12%), the reason being that it yields lower hydraulic conductivity and better compaction properties than if lower water ratio is used. This means that the model corresponding to material B is applicable to the field conditions. However, the calculations in chapter 6.4 show that the time until water saturation is too long for this material. A way to increase the rate of saturation is to apply a high pore pressure in the filter instead of 0 kPa. Two calculations with different applied water pressure, but otherwise with the same conditions and material model as the previous calculation with model B, have been done.

1000 kPa

Fig 6-5 shows history plots of the degree of saturation and the water ratio when 1000 kPa is applied in the filter mats. Water saturation is completed after about 8 months.

200 kPa

Figs 6-6 and 6-7 show results from calculations when 200 kPa is applied in the filter mats. Fig 6-6 shows contour plots of the degree of saturation after 9.5 and 19 months. Fig 6-7 shows history plots of the degree of saturation and the water ratio. Water saturation is completed after about 2 years.

6.6 Conclusions

Calculations of the saturation process with the derived material models indicate that the time until the water saturation is complete varies with the initial water ratio in the backfill. However, according to the calculations, the time until saturation is longer for a backfill with high initial water ratio than with low initial water ratio. The only difference in material model between the two backfill types is the hydraulic conductivity, which is 4 times lower for the backfill with the high initial water ratio. The difference in hydraulic conductivity is thus the regulating parameter. Since the material composition in the test probably will correspond to material type B, the time until saturation is likely to be more than 6 years. Calculations with increased water pressure for speeding up the saturation process show that about 500 kPa is required in order to reach saturation within one year.

7 Calculation of the water flow test sequence

7.1 General

After completed water saturation of the backfill sections a series of flow testing will take place. The purpose of the flow testing is to study the hydraulic function and sealing effect of the plug and the axial flow in the backfill and near field rock between the permeable mats. According to the test plan /2-1/ the flow to the mat sections will be measured after successive decrease in water pressure in the mat sections. The decrease will start at the filter on the inside of the plug and then continue to the other mats successively.

The expected water flow and water pressure distribution of such tests have been investigated in a number of hydraulic calculations with the geometry of an axial vertical section through the test site. A minor sensitivity analysis of some important parameters has also been performed.

7.2 Element mesh

The element mesh is approximately 120 m high and 240 m long. The entire mesh and a detail of the test site are shown in Fig 7-1. The structure is divided into 14 different property areas with different hydraulic properties. Fig 7-2 shows a plot of those areas. All different backfill materials and filters with the inclination 35° are modelled. The filters are inclined 35° and extend from the floor to the roof. Fig 7-2 also shows a detail of the mesh near the plug. The bentonite O-ring and a small zone between the concrete plug and the rock (for simulating a possible leakage between concrete and rock) are included in the model as well as the disturbed zone in the roof and floor and the two major vertical fractured zones in the rock.

Solid 3-D elements with the thickness 5 m have been used but with only 1 element i the ”3-direction” (perpendicular to the plane shown in Fig 7-1). This makes the cross section area of the tunnel 5x4.5=22.5 m^2 which corresponds to the real tunnel area and thus yields the correct volumetric axial water flow in the tunnel.

7.3 Material properties

The materials have been modelled as porous media. Mechanical stresses and displacements of the structure have not been included in the calculations. The hydraulic

properties of the different materials are shown in Table 7-1. The void ratio, which is also given in the table, does not influence the results of these steady state calculations.

Table 7-1. Reference hydraulic properties

Zone	*K* m/s	Void ratio *e*	Thickness *d*
1. Crushed rock	10^{-7}	0.32	
2. Backfill 30/70	10^{-9}	0.59	
3. Backfill 0/100	10^{-7}	0.32	
4. Slot filling 50/50	10^{-12}	1.0	
5. Triangular fill 20/80	10^{-9}	0.45	
6. Bentonite O-ring 100/0	$3 \cdot 10^{-12}$	1.0	
7. Concrete plug	10^{-14}	0.1	
8. Drainage layers	10^{-1}	1.0	6 cm
9. Roof, dist. zone	10^{-9}	0.003	0.3 m
10. Floor dist. zone	10^{-8}	0.003	0.7 m
11. Rock[1)]	$6 \cdot 10^{-11}$	0.0025	
12. Fractured zone, inner	$4 \cdot 10^{-8}$	0.005	3 m
13. Fractured zone, outer	$2 \cdot 10^{-8}$	0.005	0.5 m
14. Concrete/rock interface	10^{-1}	1.0	≅ 5 cm

1) The influence of the 3D-effect of the surrounding rock has been taken into account by increasing K as a function of the distance x from the test tunnel.

As noted in the table the hydraulic conductivity of the rock has been made a function of the distance from the test tunnel according to Eqn 7-1.

$$K'(x)=K(1+2x/a) \qquad (7\text{-}1)$$

where

K' = modified hydraulic conductivity

K = basic hydraulic conductivity of the rock

x = distance from the roof or floor of the tunnel

a = tunnel width (5 m)

By making the hydraulic conductivity a function of the distance from the tunnel the influence of half the rock volume according to Fig 7-3 can be taken into account (quasi 3D geometry).

7.4 Boundary conditions

Table 7-2 shows the hydraulic boundary conditions applied in the model. Calculations with a large scale rock model (chapter 8) and field measurements have shown that the water pressure in the surrounding rock is about 3 MPa. Thus, a constant water pressure of 3 MPa has been applied as boundary conditions of the outer rock boundary while zero water pressure has been applied at the inner rock boundary in the open space outside the plug.

Table 7-2. Hydraulic boundary conditions

Boundary	Boundary condition
Outer rock boundary	u = 3000 kPa
Inner rock boundary outside the plug	u = 0 kPa
Outer plug surface	u = 0 kPa

Inside the plug the boundary conditions vary with the case. In the calculation with an empty tunnel (1b) u=0 has been applied on the inner rock boundary. In the flow calculations (1d1..-1d6..) constant water pressure in some of the filters has been applied, which simulate the artificial water pressure.

7.5 Calculations

Several calculations have been made. They can be divided into the following two types:

1. Simulation of the test sequence with the reference material properties
2. ”Sensitivity analysis” for investigating the influence of applied pressure and important hydraulic properties

Table 7-3 shows summary of the different calculations. The first 8 calculations refer to the reference case while the other calculations are made after changing one of the reference parameters.

Two of the reference calculations refer to the state before start of the test sequence. Calculation 1 (After saturation) refers to the test of the function of the plug. Calculations *1mb* and *1mc* illustrate the consequence of a misfunction of the sealing of the plug. The planned test sequence is simulated in calculations *1d1* to *1d6* with lowering of the pressure in the mats to 0. The filters are numbered according to Fig 7-4. Only every second filter is studied but all filters are modelled.

Calculation *1d4u* is a repetition of calculation *1d4* but with the pressure changed to 2000 kPa instead of 0.

The rest of the calculations correspond to *1d4* but with changes in hydraulic conductivity of the 0/100 and 30/70 backfill, the disturbed zones, the inner fractured zone and the rock.

The final calculation *3d40* is a repetition of *1d4* but with a slight change in element mesh in the backfill layers and the disturbed zones. This calculation was made in order to study the influence of refining the mesh.

Table 7-3. Hydraulic modelling of the test site and the test sequences

Calculation number	Description	Changed parameter	Remark
1b	Empty tunnel		Reference case
1	After saturation		”
1d1	u=0 in filter 1		”
1d2	u=0 in filters 1-2		”
1d3	u=0 in filters 1-3		”
1d4	u=0 in filters 1-4		”
1d5	u=0 in filters 1-5		”
1d6	u=0 in filters 1-6		”
1mb	After saturation	K(o-ring)=10^{-9} m/s	Sensitivity an.
1mc	After saturation	K(o-ring)=10^{-1} m/s	”
1d4u	u=2000 kPa in filters 1-4		”
1d4c	K changed for 0/100	K(zone 1)=10^{-8} m/s	”
1d4b	K changed for 30/70	K(zone 2)=10^{-10} m/s	”
1d4rf	K changed for dist. zones	K(zone 9)=10^{-10} m/s K(zone 10)=10^{-9} m/s	”
1d4zi	K changed for fract. zone	K(zone 12)=$4\cdot10^{-7}$ m/s	”
1d4ro1	K changed for rock	K(zone 11)=10^{-11} m/s	”
1d4ro2	K changed for rock	K(zone 11)=$3\cdot10^{-10}$ m/s	”
3d40	*1d4* with finer mesh		”

7.6 Results

Some examples of results from the calculations will be given.

Empty tunnel

Calculation 1b shows that the total inflow into the test tunnel before backfilling is 2.7 l/min inside the plug and 0.1 l/min outside the plug. Since only half the rock volume is included in the calculation these figures must be doubled when compared with the measured inflow. The corresponding measured total inflow was about 5 l/min and 0,1

l/min which thus agree well with the calculations. Almost all water inflow inside the plug was achieved in the inner fractured zone both in the calculations and the measurements.

It should be noted that no skin zone was used in the calculations and that measurements made after puncturing the skin zone with 10-20 boreholes indicate that the inflow without skin zone would be at least 5 times larger. If this effect is caused by desaturation of the rock at low water pressure it means that the hydraulic conductivity of the fractured zone should be at least 5 times higher in the other flow calculations. However, an increased hydraulic conductivity of this zone does not influence these calculations much since it is high enough for providing the inner part of the tunnel with a sufficiently high water pressure (as shown in calculation *1d4zi*).

After completed water saturation

After water saturation the plug is supposed to keep the water pressure high inside the plug. Calculation *1* yields the hydraulic situation when the plug is sealed properly by the bentonite o-ring (reference case). Fig 7-5 shows the results of the calculation. Since the concrete/rock interface is completely untight almost the entire pressure decrease is taken by the bentonite o-ring (about 2.6 MPa) and only a small part (about 0.4 MPa) is taken by the 30/70 backfill. The water flow to the outside of the plug (including 1m tunnel outside the plug) is 0.014 l/min.

Plug with reduced sealing capacity

Fig 7-6 shows the results of calculations simulating a less effective plug sealing with a hydraulic conductivity of 10^{-9} m/s of the bentonite in the o-ring (*1mb*) and 10^{-1} m/s (*1mc*). For K=10^{-9} m/s the water pressure inside the plug is reduced to about 1.7 MPa and the rest of the pressure drop taken by the 30/70 backfill. The water flow to the outside of the plug is 0.066 l/min.

For K=10^{-1} m/s there is no sealing effect of the plug. Fig 7-6 shows that practically the entire pressure decrease is taken by the 30/70 backfill. The sealing effect of 0/100 backfill is very small. The water flow to the outside of the plug is 0.184 l/min. The outflow is in spite of the inefficient plug quite low due to the sealing power of the 30/70 backfill. These calculations show that the pressure drop over the plug is a better measure of the sealing efficiency of the plug than the flow and that an artificially applied pressure inside the plug may be required for a proper evaluation.

Reference cases of flow testing

The calculation of the flow test sequence with gradually application of zero pressure in the filter mats have yielded the following results:

Calculations *1d1* to *1d3* yields a water pressure distribution that is very similar to calculation *1mc* since there is no sealing effect of the 0/100 backfill. Figure 7-7 shows the water flux ($m^3/s,m^2$) in calculation *1d1*, where zero water pressure is applied in the filter on the inside of the plug. Fig 7-7 also shows the water flux into the filter as a function of the distance from the roof. These plots show that water flows from the inner fractured zone through the crushed rock to the floor. The flow in the sections with 30/70

backfill goes mainly in the floor of the rock and the flow in the sections with 0/100 backfill goes mainly in the backfill. The flow into the filter on the plug wall goes in the lower part since the upper triangular section is filled with 20/80 backfill with low hydraulic conductivity.

Calculation *1d4* simulates the flow test when zero water pressure is applied in the filter between the two backfill types. This case is also used for the sensitivity analyses in the rest of the calculations. Fig 7-8 shows the water pressure distribution, Fig 7-9 shows the flux and Fig 7-10 shows the water flow into the filter. 0.4 m of the filter will be folded and attached to the rock in both the roof and the floor in the field test. This is modelled by applying u=0 not only in the filter but also in the first node towards the plug (to the right in the figures) in the floor and the roof. Fig 7-8 shows that the water pressure distribution in the backfill section is evenly distributed and that the iso-pressure lines are parallel to the filter, which should yield an evenly distributed inflow. Figs 7-9 and 7-10 confirm this with the exception of close to the floor and roof where the inflow is higher due to the geometry (in the roof) and the higher hydraulic conductivity in the floor.

The results from calculations *1d5* and *1d6* are similar to the results of calculation *1d4* but the inflow into the filter mat is higher since the hydraulic gradient is higher. Fig 7-11 shows the pore water pressure distribution and the inflow distribution in filter 5.

”Sensitivity analysis”

Calculations *1d4u - 1d4ro2* are made with the purpose to try to see how sensitive the water pressure distribution and the water inflow into the filters are to the hydraulic conductivity values of the different parts in the model.

Calculation *1d4u,* simulates that the water pressure in all the filters are lowered to 2 MPa instead of to 0 MPa. The actual flow testing will probably start with such a program in order to avoid piping and to investigate a possible water pressure dependency. The results of the calculations show that the pressure gradient and the flow are proportional to the decrease in water pressure.

Calculation *1d4c* shows the influence of the hydraulic conductivity of the crushed rock in the inner part of the tunnel (zone 1). The calculation, which is made with a hydraulic conductivity that is a factor of 10 lower than in the reference case, shows that there will be some sealing potential in this material. This yields a slightly lower water pressure gradient in the backfill sections and thus a lower inflow into the filter. A 20% decrease in the inflow was reached for this case. The calculation shows that it is important to have a material with sufficiently high hydraulic conductivity in the inner part.

Calculation *1d4b* shows the influence of the hydraulic conductivity of the 30/70 backfill. In this calculation the hydraulic conductivity is lowered with a factor of 10. Figs 7-12 to 7-14 show the results. The hydraulic gradient is increased but not very much. The flow pattern is changed. More flow goes in the floor and the inflow into the central part of the filter is decreased with a factor of 8-9. The results indicate that the average hydraulic conductivity in the central part of the backfill sections should be easily evaluated.

Calculation *1d4rf* shows the influence of the hydraulic conductivity of the disturbed zones in the roof and the floor. The hydraulic conductivity of these parts have been reduced with a factor of 10. Figs 7-15 to 7-17 show the results. There is a small increase in hydraulic gradient similar to the one reached when the hydraulic conductivity of the 30/70 backfill was reduced. There is a large decrease in flow in the floor resulting in a strong reduction in inflow in the lower part of the filter. The inflow into the central and upper part of the filter is about the same as for the reference case, which confirms that it is the geometry that causes the large inflow in the filter close to the roof.

Calculation *1d4zi* shows the influence of the hydraulic conductivity of the inner fractured zone. Fig 7-18 shows the results of this calculation where the hydraulic conductivity of this zone have been increased with a factor of 10. The calculation shows that the water pressure is slightly increased in the crushed rock compared to the reference case, which yields an increase in hydraulic gradient of about 5% and an increase in inflow also with about 5%. The conclusion is that the hydraulic properties of the fractured zone is not very important as long as the supply of water is enough to keep a high water pressure in the inner part of the tunnel.

In calculations *1d4r01* and *1d4r02* the influence of the hydraulic conductivity of the surrounding rock has been studied by decreasing it with a factor 6 and increasing it with a factor of 5 compared to the reference case. The resulting change in water pressure is small. The total difference between these two calculations (which have a difference in hydraulic conductivity of the rock of a factor of 30) is a difference in hydraulic gradient of 15% and a resulting difference in water inflow into the filter of also 15%. Fig 7-19 shows the calculated inflow from the two calculations. The difference in peak flow close to the roof and floor is somewhat higher.

The element mesh in the model is rather coarse in the disturbed zones and in the backfill sections. In order to see if this has any significant influence on the calculated results the mesh was refined and calculation *1d4* repeated (*3d40*). Fig 7-20 shows the element mesh in the near field area together with the calculated water pressure and flow distributions. Fig 7-21 shows the calculated inflow into the filter. If these results are compared with the corresponding results of calculation *1d4* (Figs 7-8 to 7-10) the following observations can be made:

- The difference in water pressure in the interesting parts is insignificant
- There is a small difference in flow pattern in the floor
- The inflow into the central part is identical but the peak values close to the roof and floor are higher and less wide in the calculation with the refined mesh.

A finer element mesh thus captures the detailed behaviour better but does not influence the overall behaviour.

Flow rate

The inflow into the filters must be high enough to be measurable. The inflow into a central filter will for the reference case be about 3.6 l/h in filter 4. If 2 MPa water pressure is applied in the filters instead of 0 MPa and if the hydraulic conductivity of the

30/70 backfill is only 10^{-10} m/s the inflow will be about 0.12 l/h. This flow is low but clearly measurable.

7.7 Conclusions

The system that is modelled is complex with several materials which have a hydraulic conductivity that is not very well known. The calculations indicate that some of these materials can in some cases ”disturb” the evaluation of the results. It is important that the system is not so ambiguous that it is impossible to evaluate the important parameters. The following preliminary conclusions can be drawn from these calculations:

- The influence of the properties of the inner fractured zone and the inner drainage material of crushed rock is not very large as long as the transmissivity is high enough to supply the inner part of the tunnel with a high pressure. This seems to be the case for this system and the pressure measurements will reveal if this is not the case.

- The undisturbed unfractured surrounding rock has only a small influence on the results. The reason is that the hydraulic conductivity is assumed to be much lower than the hydraulic conductivity of the backfill and the disturbed zones.

- The hydraulic conductivity of the disturbed zones are important for the water pressure in the backfill inside (to the left of) the inner pressure regulated filter (u=0) and the water inflow into the parts of the filter that are located close to the rock. A preliminary conclusion is that it will be difficult to distinguish between the flow in the backfill and disturbed zones if the hydraulic conductivity of the disturbed zones is lower or equal to the hydraulic conductivity of the backfill. If the hydraulic conductivity of the disturbed zones is higher it should be shown in the tests since one filter is split into 3 parts in the field test (one part close to the roof, and part close to the floor and one large part in the centre). However, it is of course not possible to distinguish a high hydraulic conductivity in the disturbed zone from a leakage in the backfill close to the rock.

- The average hydraulic conductivity of the central part of the backfill seems to be possible to evaluate in a reliable way since this is measured in a separate filter.

- The inflow rate into the filters seems to be high enough to be possible to measure.

8 Large scale 3D model

8.1 General

The results and evaluation of the water flow tests /2-1/ are strongly influenced by the hydrology of the surrounding rock mass and the geometry of the excavations close to the test site. In order to understand the hydraulic function of the surrounding rock and generate proper boundary conditions for the small scale models, a large scale 3D model of the test site and the surrounding rock and excavations have been made. The hydro-geological background for the model is given in /8-1/ but the fractured zones have not been included in the present model.

8.2 Element mesh

The element mesh is composed of 12x22x23=6072 elements forming a box with the approximate dimension 200x200x200 m^3. Figs 8-1 and 8-2 show the element mesh from outside and the modelled excavations. The assembly hall (for the TBM machine) and the inclined TBM tunnel can be seen in Fig 8-2 as well as the test tunnel (ZEDEX tunnel) and the Demonstration tunnel. The test tunnel is located between the TBM tunnel and the Demonstration tunnel. All excavations are modelled with rectangular cross sections.

8.3 Material properties

The model has only been used for hydraulic calculations. Since the original ABAQUS elements for porous media flow calculations are hydro-mechanical and thus also include mechanical properties, the elements have been mechanically constrained.

The following average value of the hydraulic conductivity K_r has been used for the rock:

$K_r = 5 \cdot 10^{-10}$ m/s

This value is only affecting the flow rate and not the magnitude of the water pressure. The flow rate is directly proportional to the hydraulic conductivity.

No fractured zones have been included in the model. The calculated water pressure distribution around the excavations showed that a decreased hydraulic conductivity around the tunnels (a skin zone) is required in order to have a water pressure distribution that resembles the measured distribution. Such a skin zone was included around the test tunnel and in the roof, floor, and wall on the tunnels adjacent to the test tunnel. Fig 8-3

shows the location of those skin zones. The zones were made with a thickness of 3 m and with the following hydraulic conductivity K_s:

$K_s = K_r/4$

Since no transient calculations were made the hydraulic conductivity is the only parameter that has an influence on the results.

8.4 Calculations

Description

Six calculations have been done. Three different sets of boundary conditions and two different hydraulic conductivity reduction factors S_f have been used. They are described in Table 8-1 where

$S_f = K_s/K_r$

Boundary 1: Upper horizontal surface

Boundary 2: Lower horizontal surface

Boundary 3: Vertical surfaces parallel to the axis of the test tunnel

Boundary 3: Vertical surfaces perpendicular to the axis of the test tunnel.

Table 8-4 Boundary conditions and hydraulic conductivity reduction factor S_f used in the different calculations.

Calculation	S_f	Boundary 1	Boundary 2	Boundary 3	Boundary 4
a11	1	u=3200 kPa	No flow	No flow	No flow
a12	1	u=3200 kPa	u=5200 kPa	No flow	No flow
a13	1	u=3200 kPa	u=5200 kPa	u=hydrostatic	No flow
a21	0.25	u=3200 kPa	No flow	No flow	No flow
a22	0.25	u=3200 kPa	u=5200 kPa	No flow	No flow
a23	0.25	u=3200 kPa	u=5200 kPa	u=hydrostatic	No flow

At the inner rock surface of the excavations a constant water pressure of u = 0 kPa has been applied in all calculations

Influence of boundary conditions

The calculated water pressure at the boundaries from calculations *a22* and *a23* is shown in Fig 8-4. A comparison has been made with calculations made in a regional scale that includes several km^2 /8-2/. Fig 8-5 shows the water pressure as a function of depth from

that calculation at two vertical lines in the centre of the two planes defining boundary 3 (see Table 8-4). Fig 8-5 shows that the water pressure at that boundary is almost hydrostatic (minus about 30 kPa) which means that the boundary conditions used in calculations *a13* and *a23* are the most relevant ones.

Influence of skin zone

The results of calculations *a13* and *a23* are shown in Figs 8-6 and 8-7. The influence of the skin zone around the test tunnel is clearly seen. The pressure midway between the test tunnel and the demonstration tunnel or the TBM tunnel is about 600 kPa if $S_f = 1$ or no skin is used (*a13*) and about 1000 kPa with $S_f = 0.25$ (*a23*). Preliminary measurements show that the water pressure close to the excavations is even higher indicating an even lower hydraulic conductivity reduction factors..

Water pressure and inflow results

The most relevant calculation is thus calculation *a23* which has the most regulated boundary conditions and a hydraulic conductivity reduction factor of 0.25. The resulting water pressure distribution is shown in Fig 8-8, which shows a detail of Fig 8-7.

The water inflow into the test tunnel was for this calculation 5.2 l/h which is very close to the measured inflow.

8.5 Conclusions

The preliminary large scale 3D model described in this chapter have yielded the following conclusions:

- The hydrology of the rock surrounding the test tunnel can be modelled in this scale
- The model should include a skin zone with decreased hydraulic conductivity around all the excavations
- The hydraulic boundary conditions should be defined with constant pressure boundaries for at least those boundaries defined in calculation *a23*.
- The average hydraulic conductivity of the rock around the test tunnel is $5 \cdot 10^{-10}$ m/s. However, the model should include the major fractured zones intersecting the test tunnel in order to properly model the heterogeneity of the rock. Such a model will result in a very non-uniform inflow.
- The next step is to make a model that includes three fractured zones and a skin zone around all excavations. The values of the hydraulic conductivity will be calibrated with measured inflow and water pressure distributions. The model will also be used to simulate the effect of the plug and some of the flow tests.

References

/2-1/ **Börgesson L 1997.** Äspö Hard Rock Laboratory. Test Plan for Backfill and Plug Test. SKB Progress Report HRL-98-08

/4-1/ **Hibbitt, Karlsson, and Sorensen -** ABAQUS manuals, HKS Inc.

/5-1/ **Börgesson L, Johannesson L-E & Sandén T 1998.** Backfill materials based on crushed rock (part 2). Geotechnical properties determined in the laboratory. SKB Progress Report HRL (in press).

/8-1/ **Stenberg L & Gunnarsson D 1998.** Äspö Hard Rock Laboratory. Characterisation of the ZEDEX drift in advance to the Backfill and Plug Test. SKB Progress Report HRL-98-10

/8-2/ **Svensson U 1997.** A site scale analysis of groundwater flow and salinity distribution in the Äspö area. SKB Technical Report 97-17

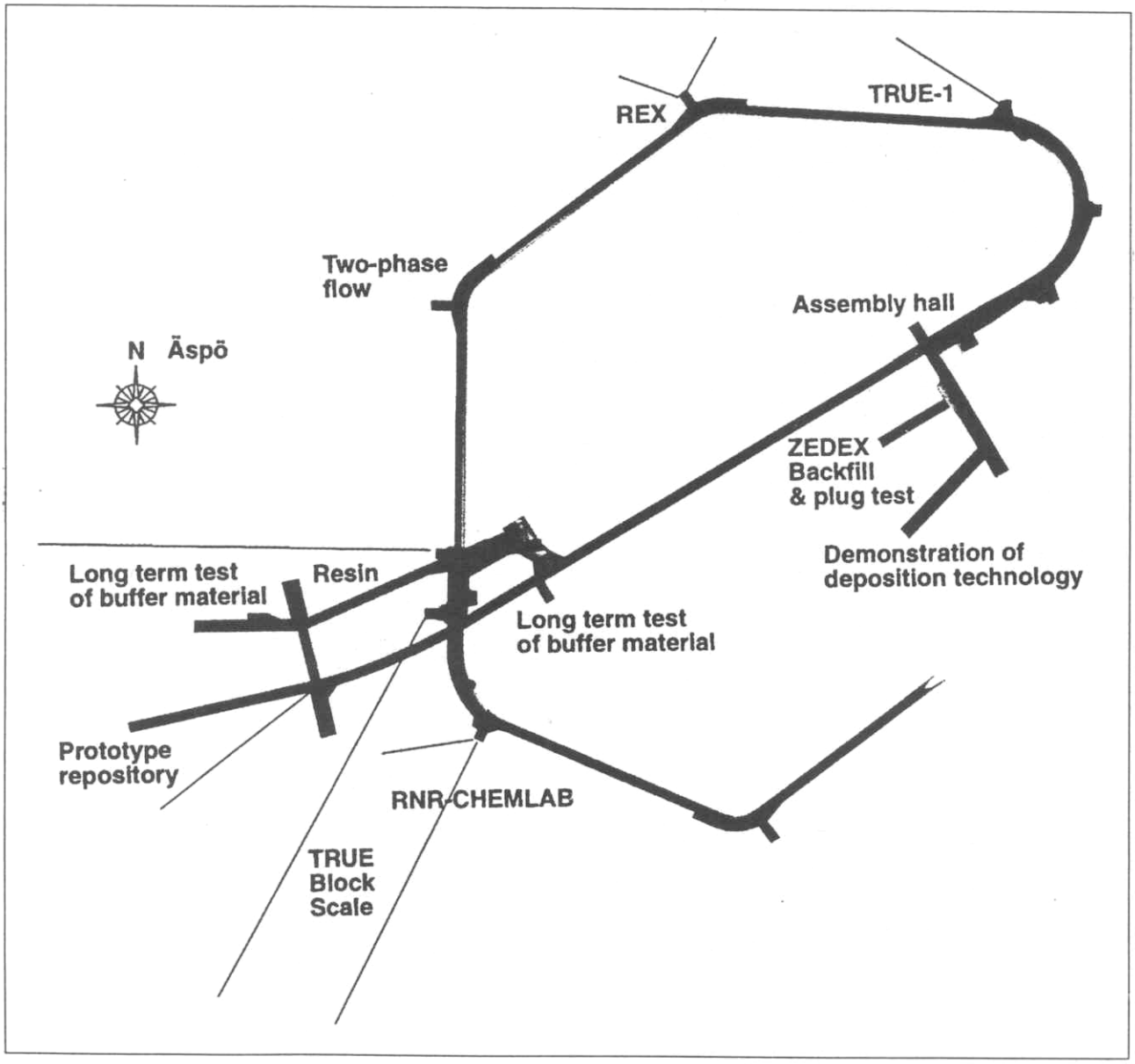

Figure 2-1. Location of the Backfill and Plug Test in Äspö HRL

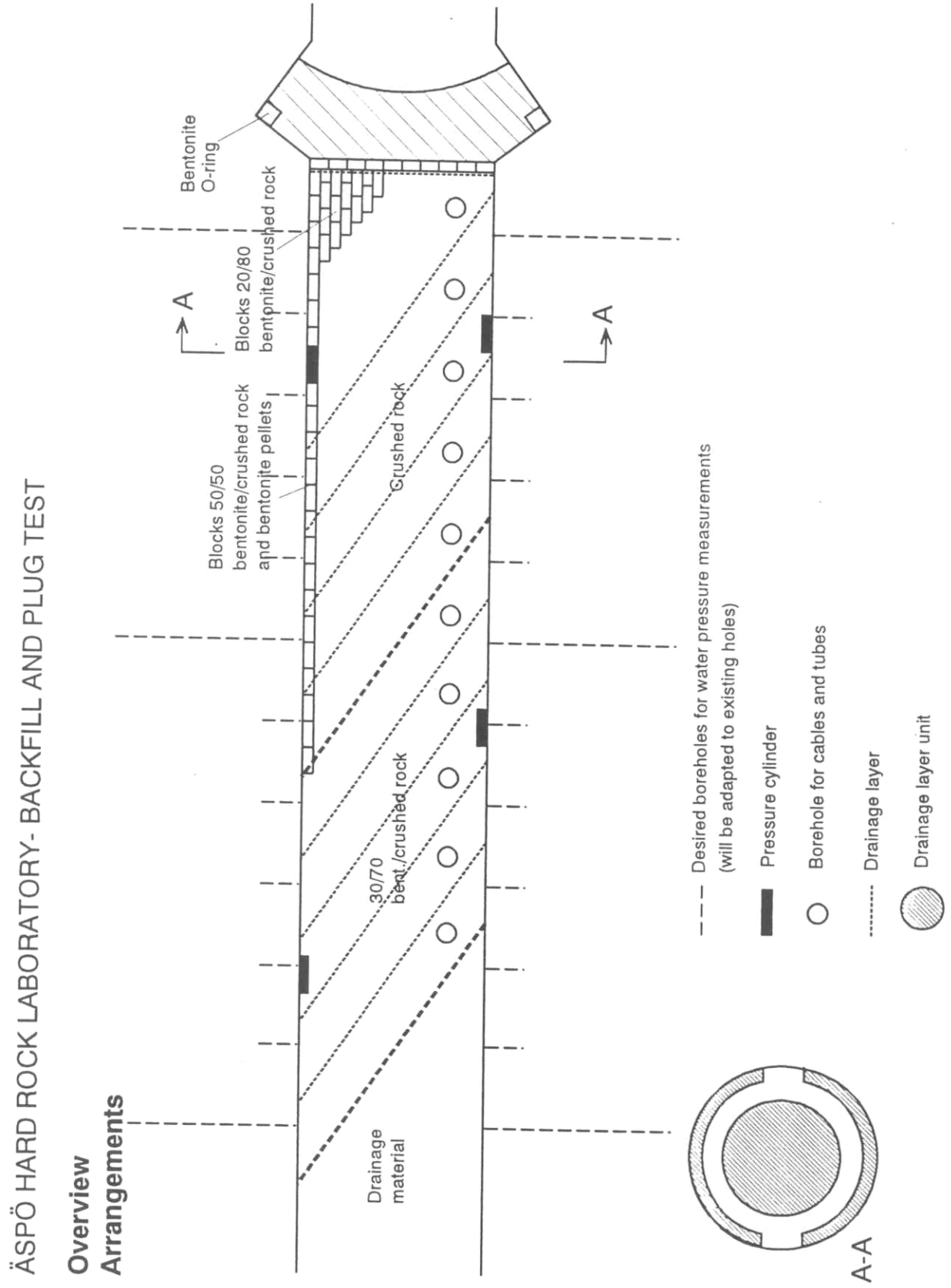

Figure 2-2. An overview of the test facilities in the Backfill and Plug Test

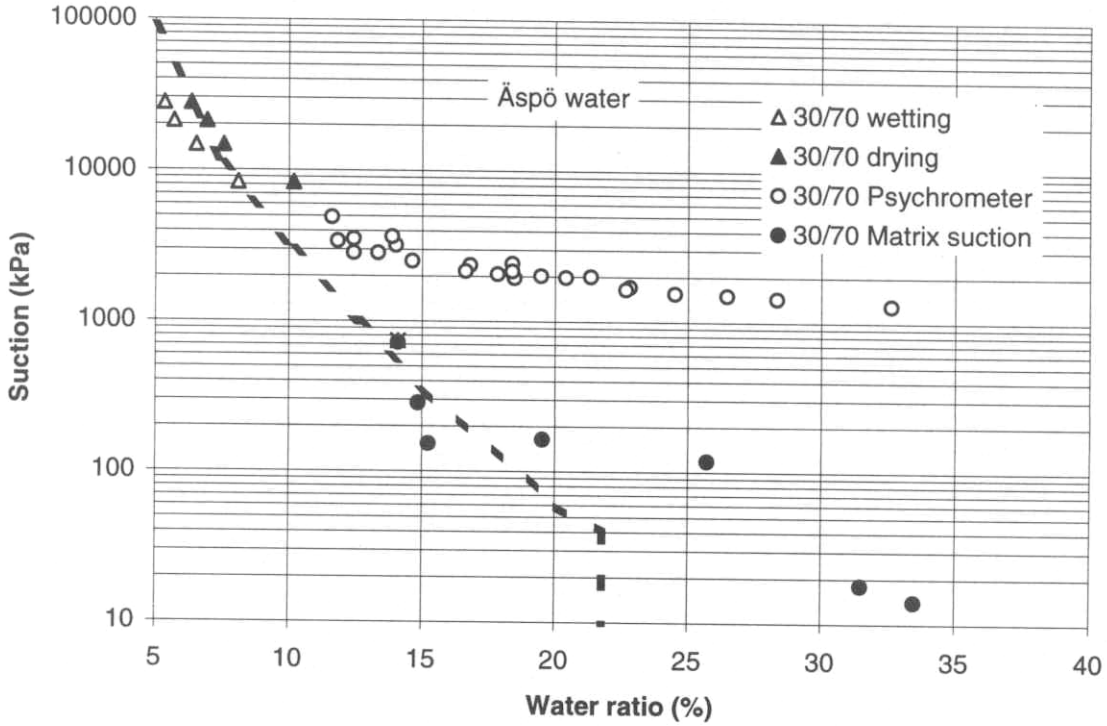

Figure 5-1. Measured relation between matric suction and water ratio of the reference 30/70 backfill material (filled circles) and the relation used in the calculations (dashed line). The other symbols correspond to total suction.

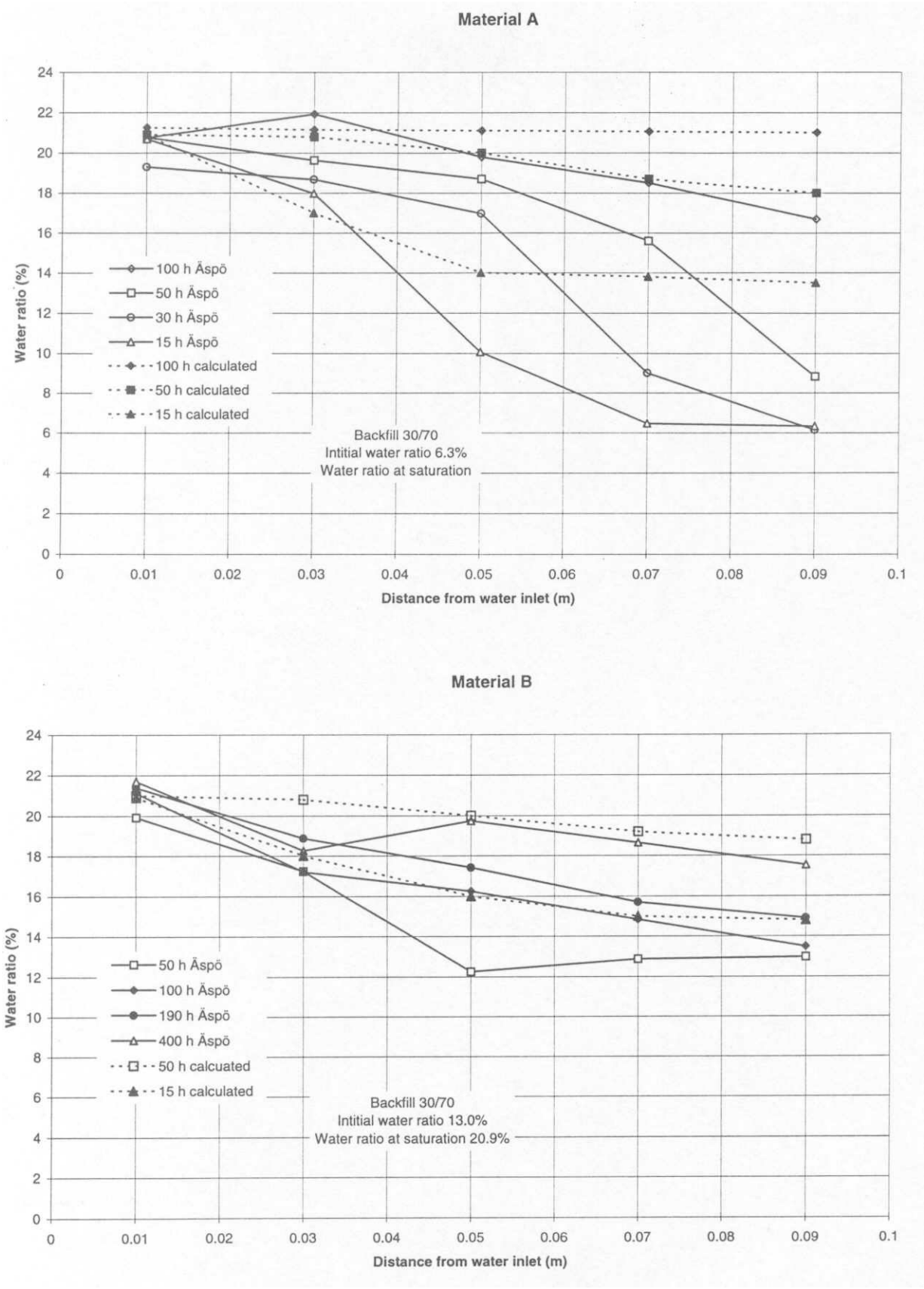

Figure 5-2. Calculated and measured water ratio as a function of the distance from the water inlet for material A (upper) and material B (lower) before calibration of the material model.

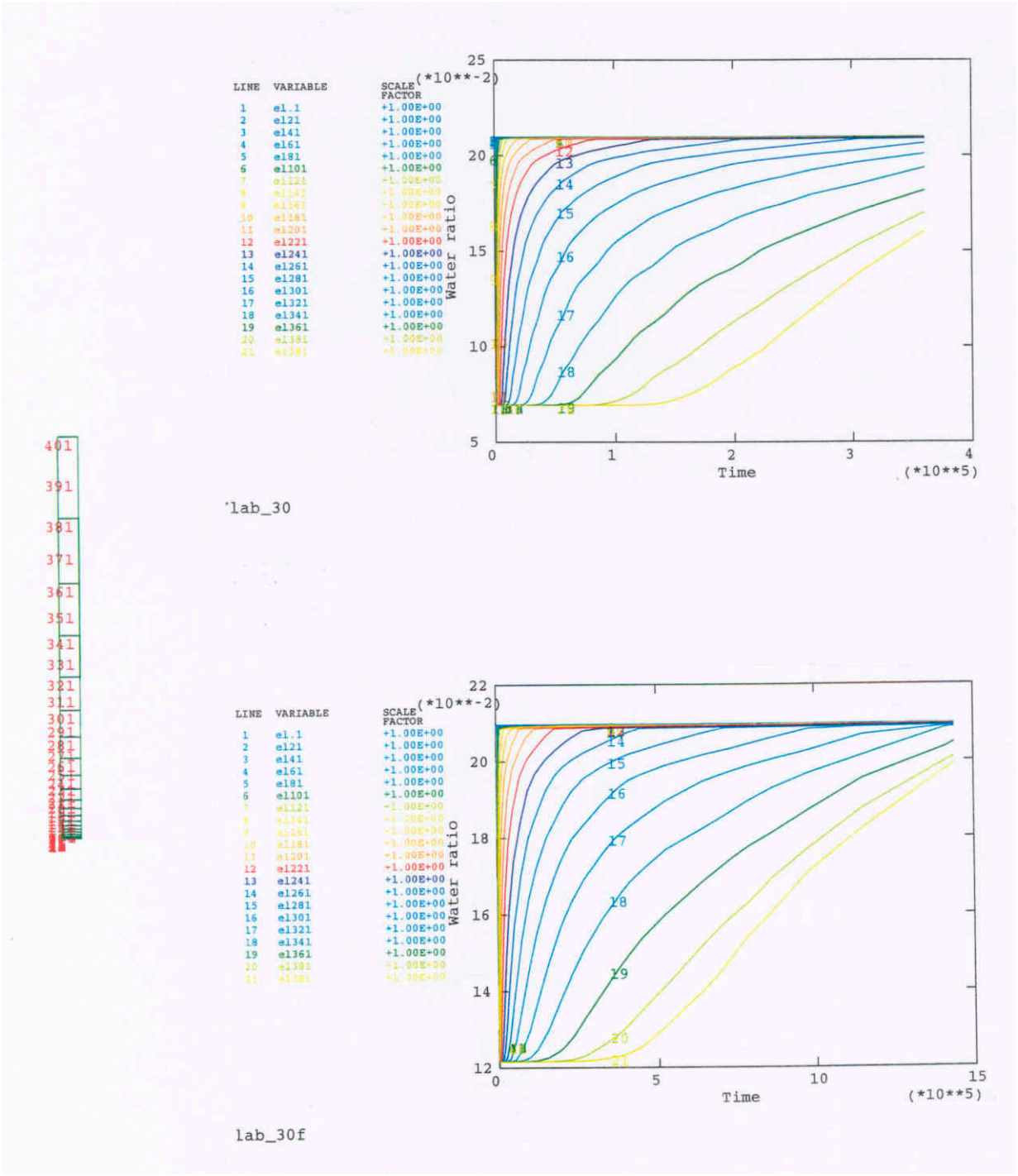

Figure 5-3. Element mesh for the laboratory test calculation and the change in water ratio with time (s) for material A (upper) and material B (lower).

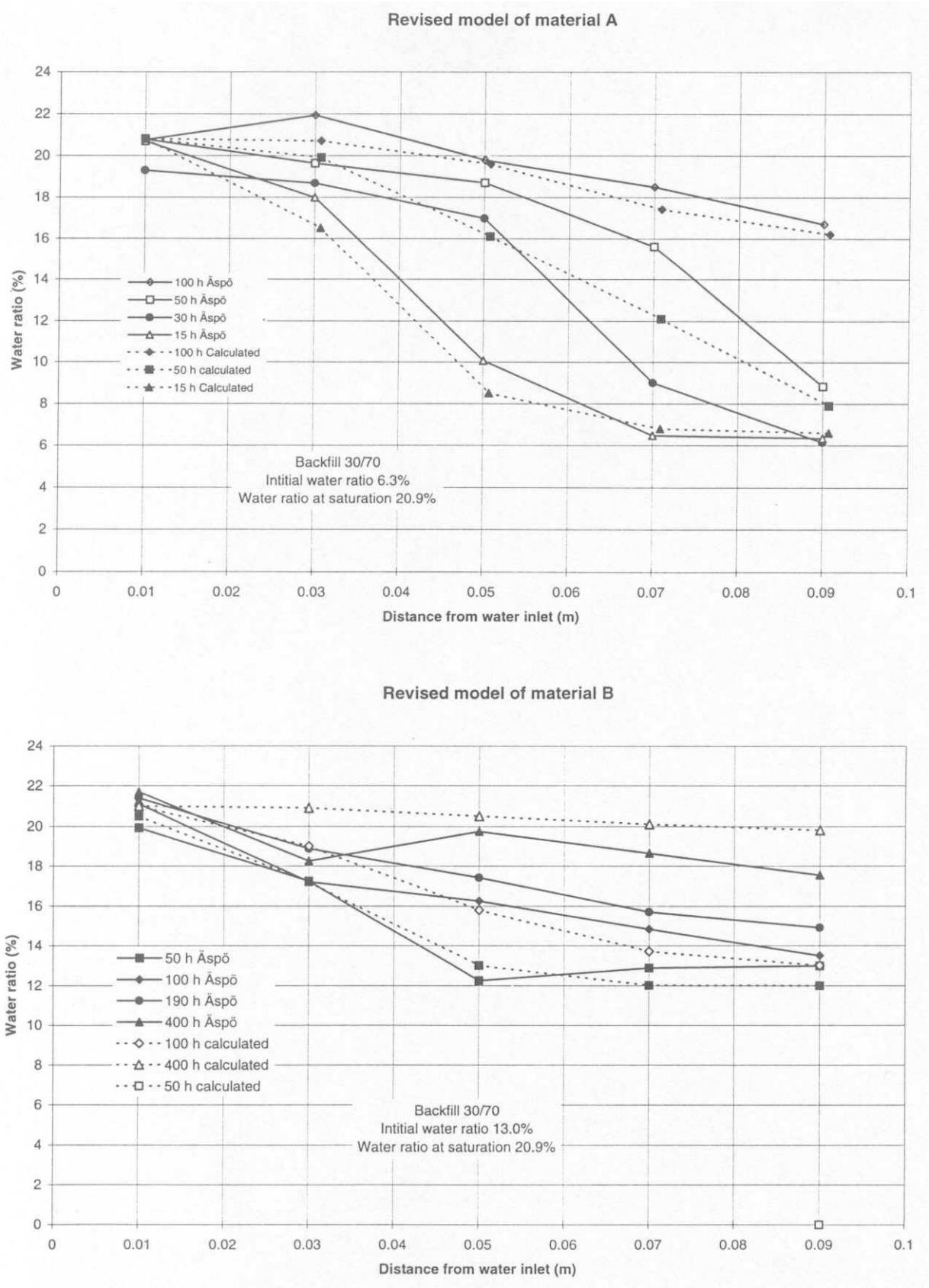

Figure 5-4. Calculated and measured water ratio as a function of the distance from the water inlet for material A (upper) and material B (lower) after calibration of the material model.

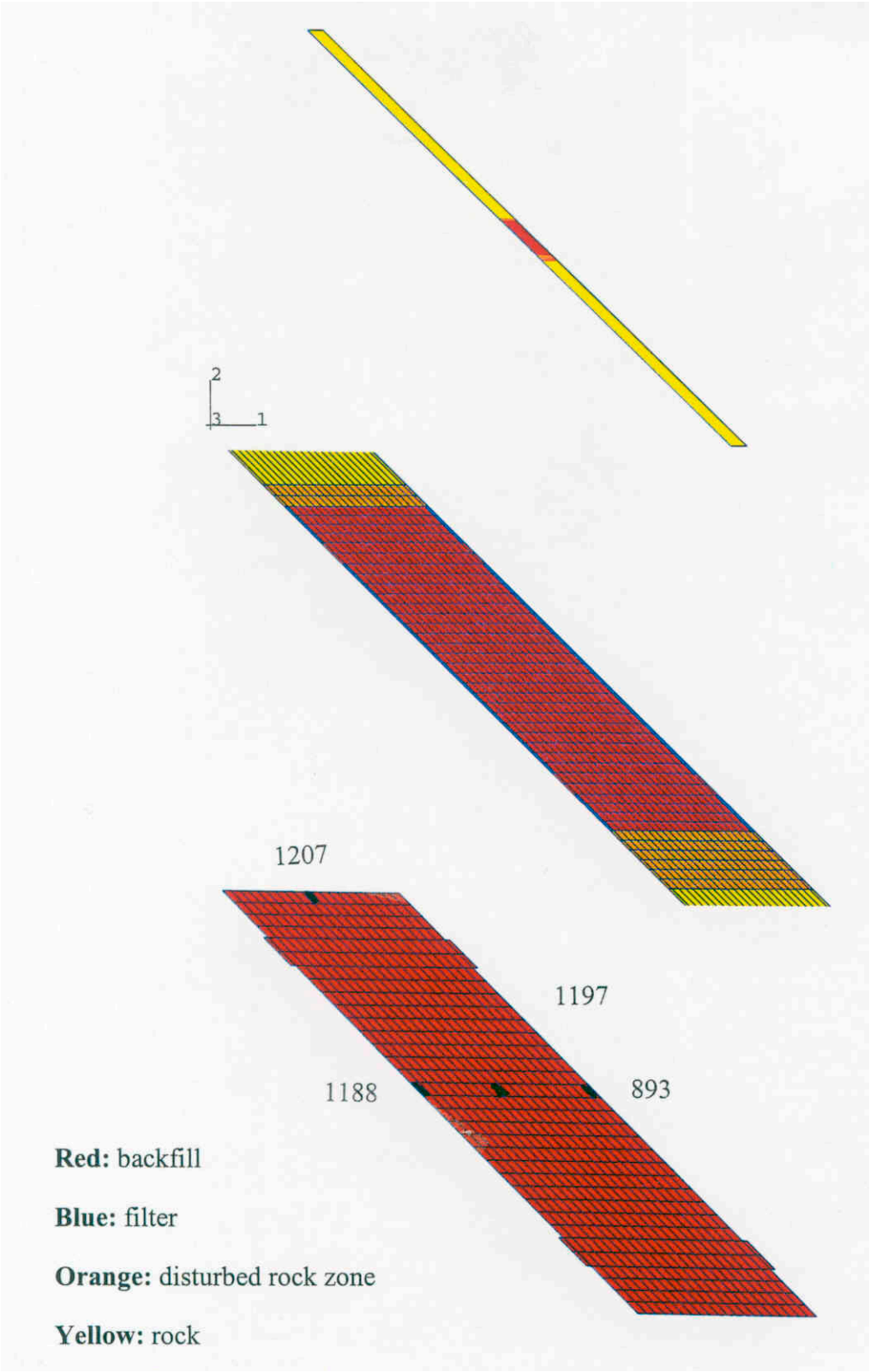

Figure 6-1. Element mesh for the calculation of the saturation process. The upper figure shows the entire model, the central figure shows the mesh close to the backfill, and the lower figure shows the mesh of only the backfill.

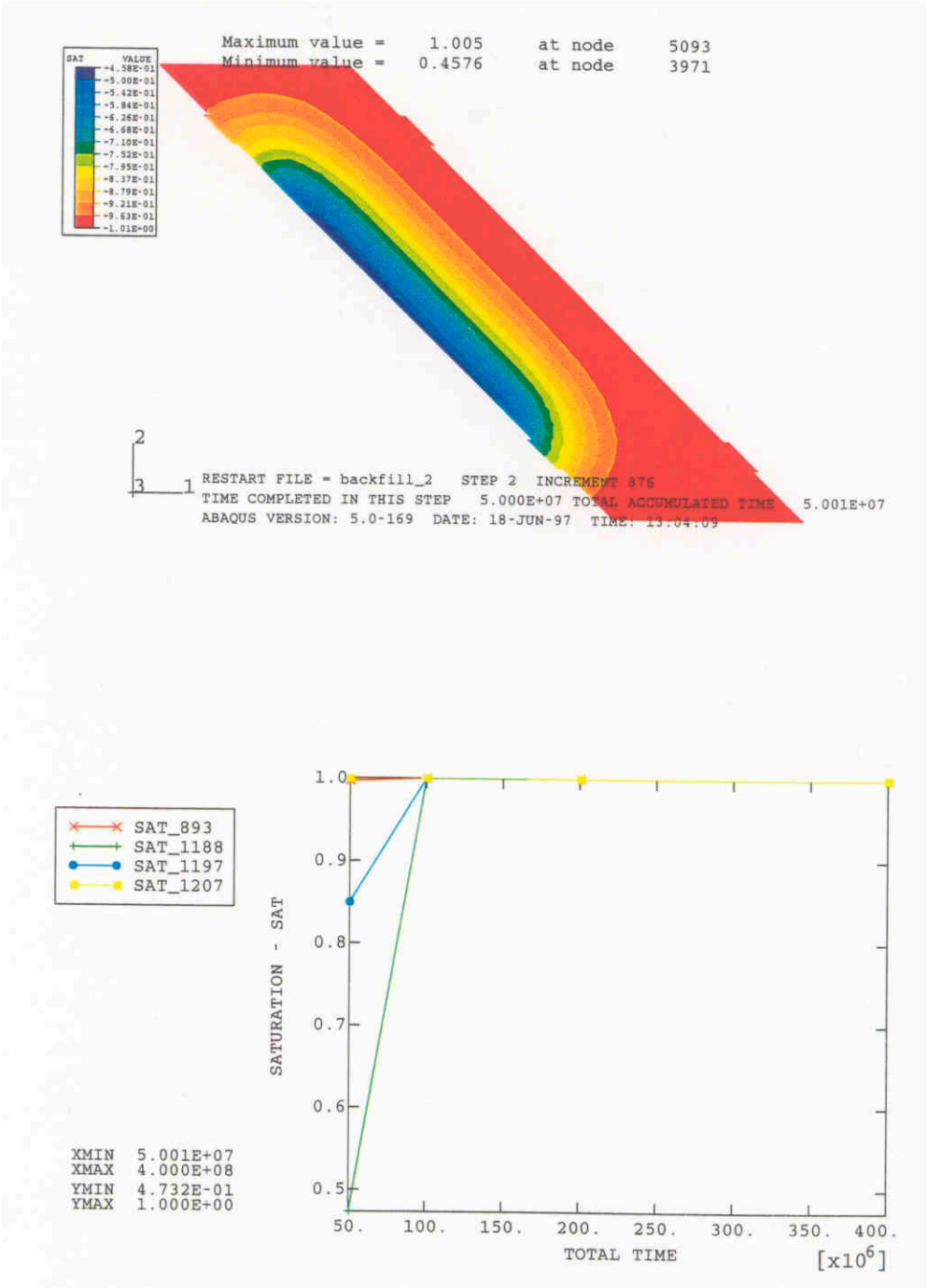

Figure 6-2. Material A with w_0=6.3%. Calculated degree of saturation after 1.6 years (upper) and as a function of time for the 4 points in the backfill shown in Fig 6-1. Green: left centre. Blue: middle centre. Red: right centre.

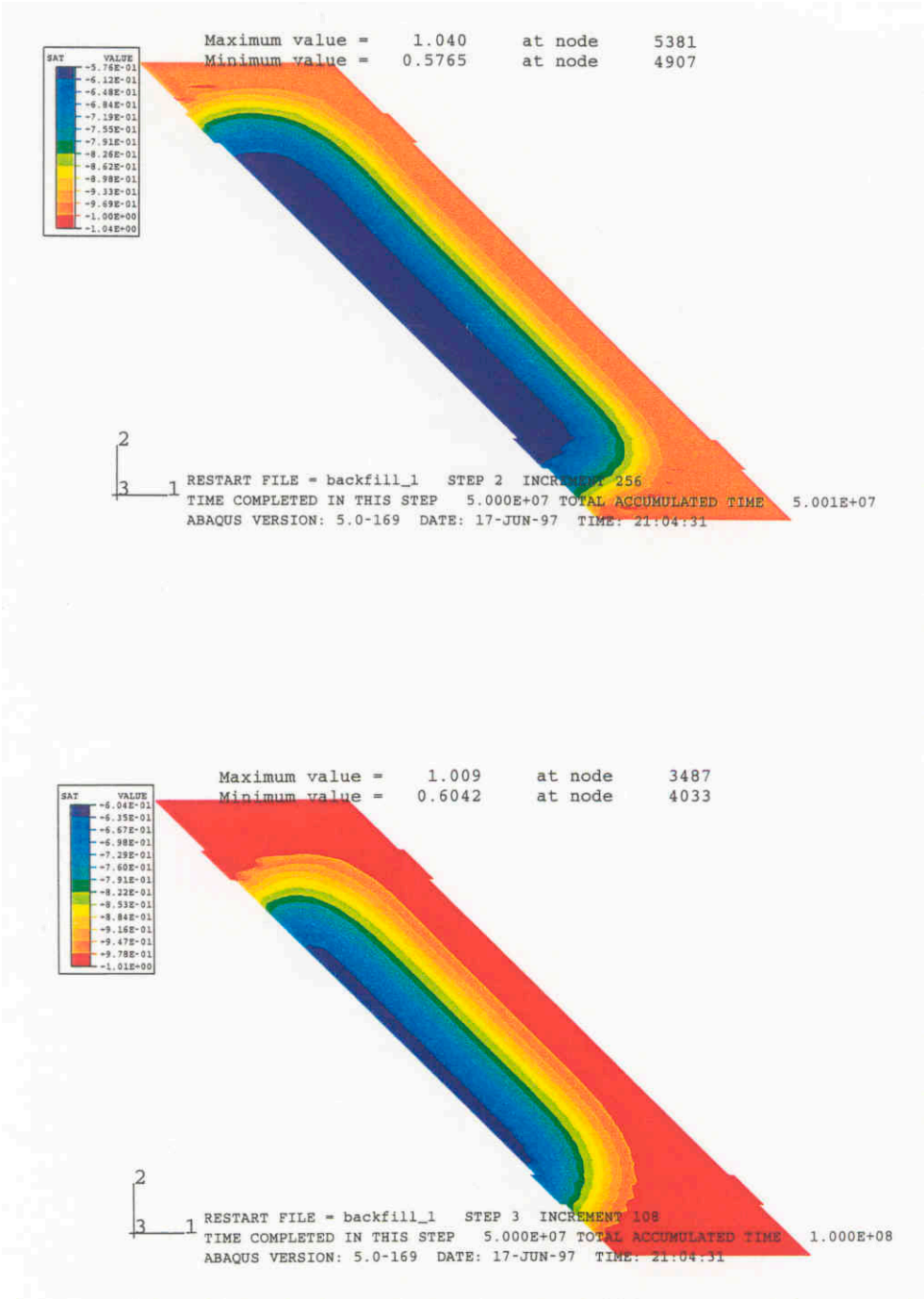

Figure 6-3. Material B with w_0=12.0%. Calculated degree of saturation after 1.6 years (upper) and 3.2 years.

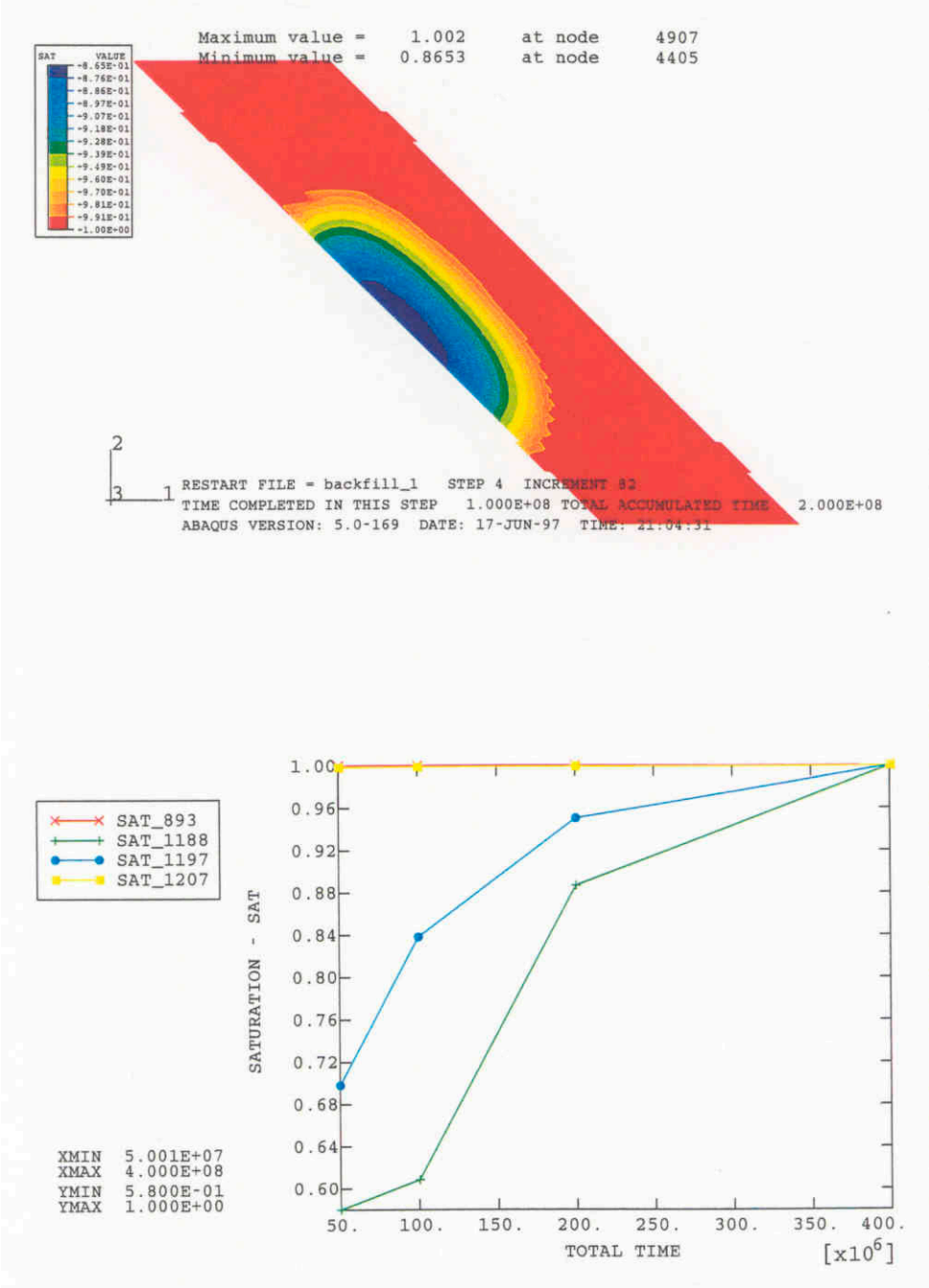

Figure 6-4. Material B with w_0=12%. Calculated degree of saturation after 6.3 years (upper) and as a function of time for the 4 points in the backfill shown in Fig 6-1. Green: left centre. Blue: middle centre. Red: right centre.

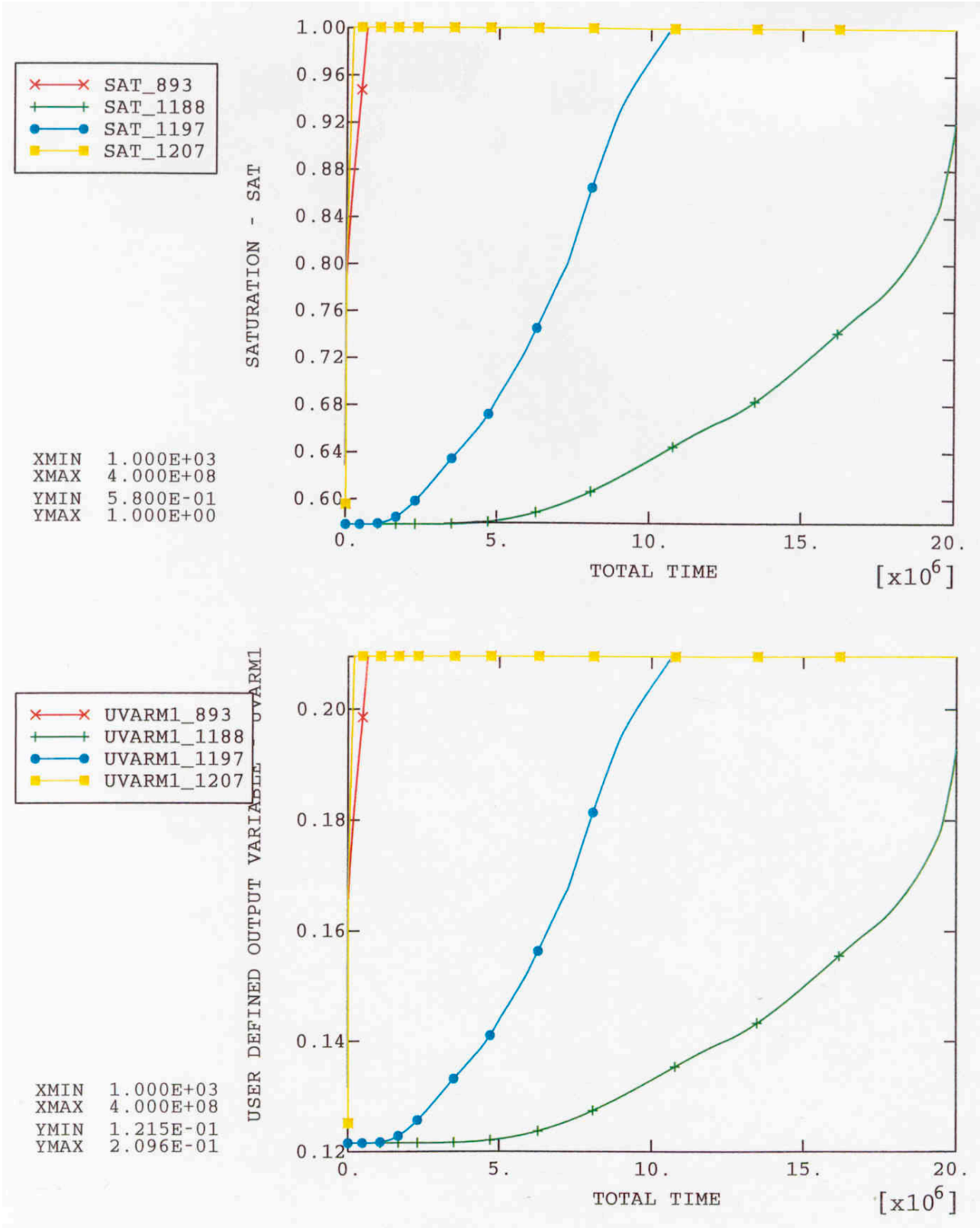

Figure 6-5. Results of calculations with 1000 kPa water pressure applied in the filter mats (material B). Degree of saturation (upper) and water ratio as a function of time for the 4 points in the backfill shown in Fig 6-1. Green: left centre. Blue: middle centre. Red: right centre.

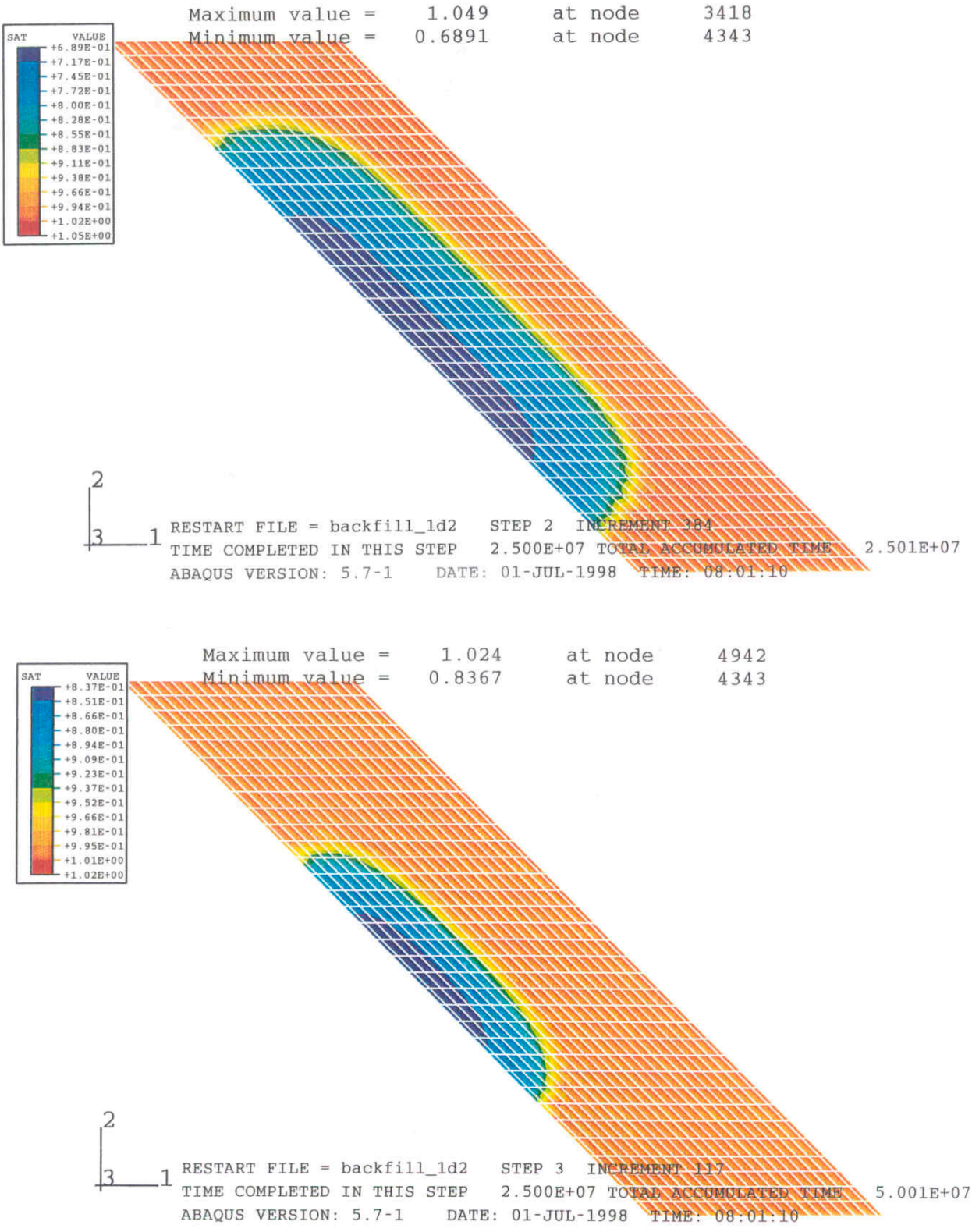

Figure 6-6. Results of calculations with 200 kPa water pressure applied in the filter mats (material B). Degree of saturation after 9.5 months (upper) and 19 months.

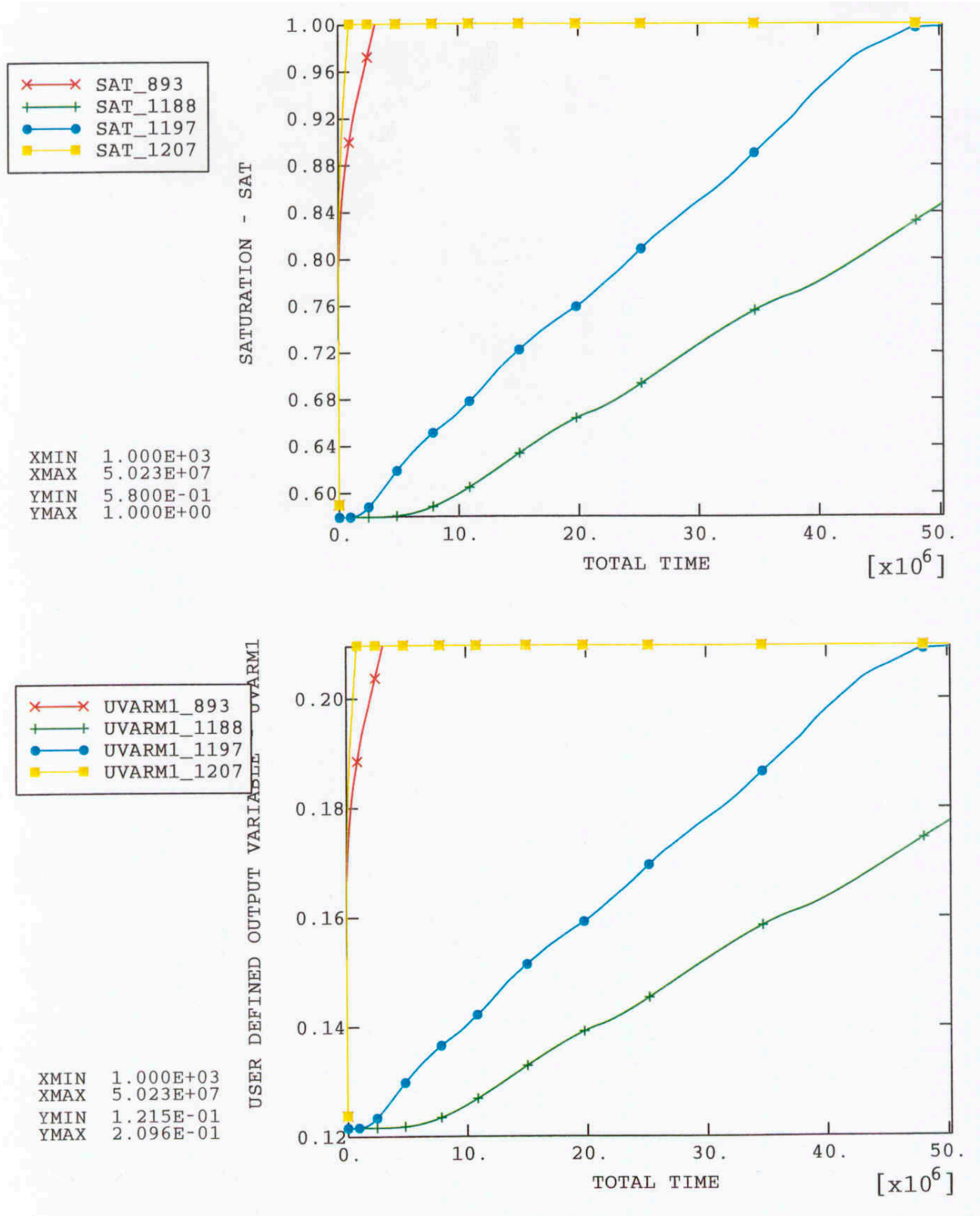

Figure 6-7. Results of calculations with 200 kPa water pressure applied in the filter mats (material B). Degree of saturation (upper) and water ratio as a function of time for the 4 points in the backfill shown in Fig 6-1. Green: left centre. Blue: middle centre. Red: right centre.

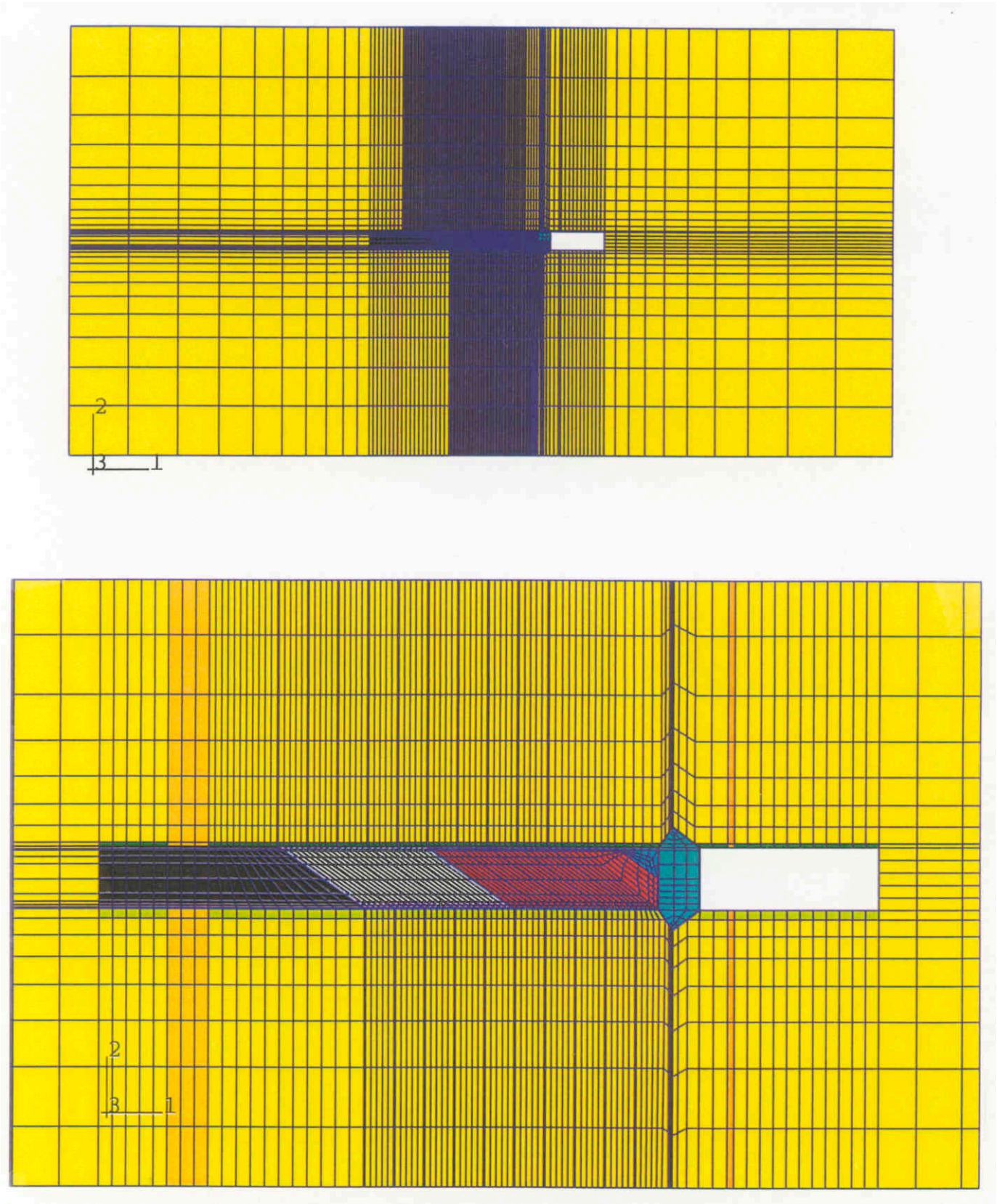

Figure 7-1. The entire element mesh used for the hydraulic simulation of the test sequences and a detail of the test site.

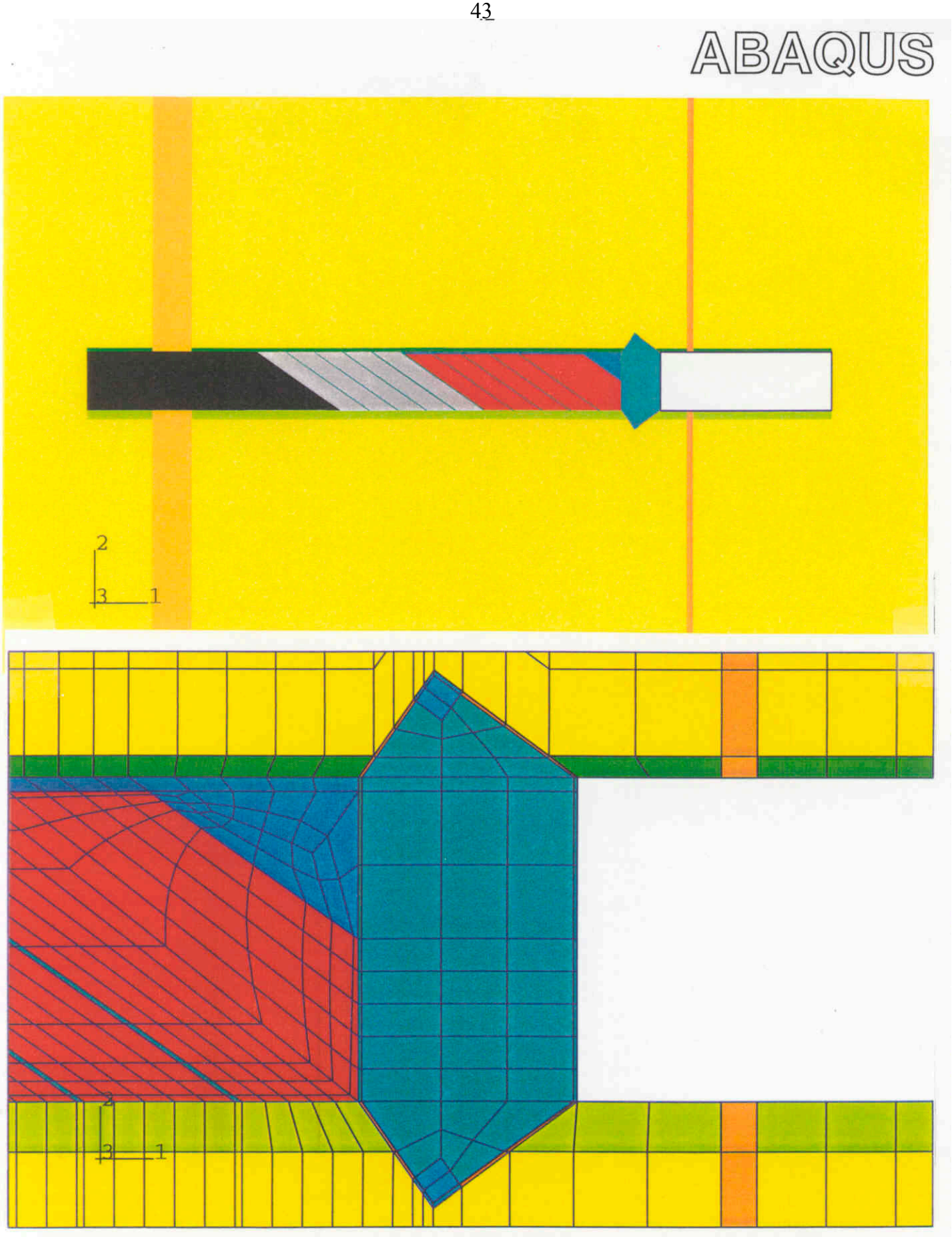

Figure 7-2. The property areas in the model and a detail of the mesh at the plug.

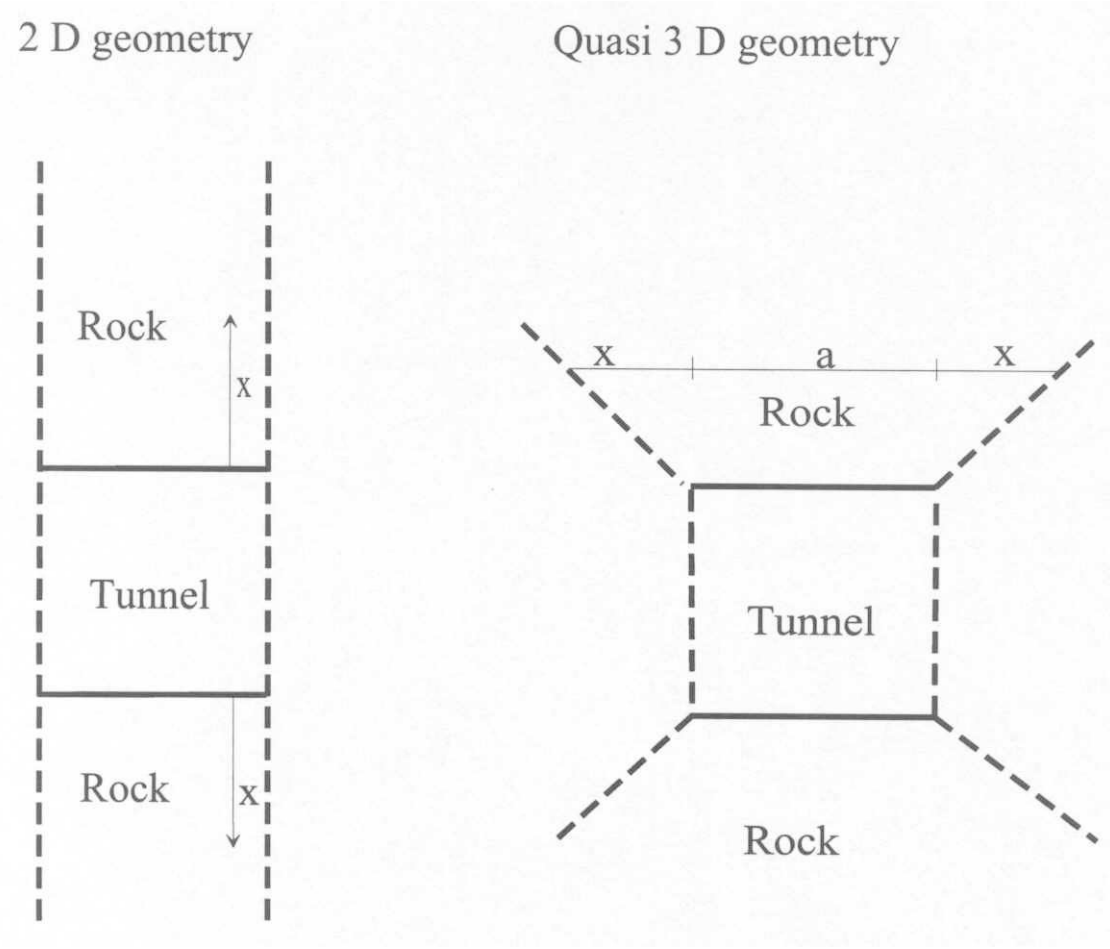

Figure 7-3. The influence of half the rock volume has been taken into account by simulating a quasi 3D geometry according to the right drawing.

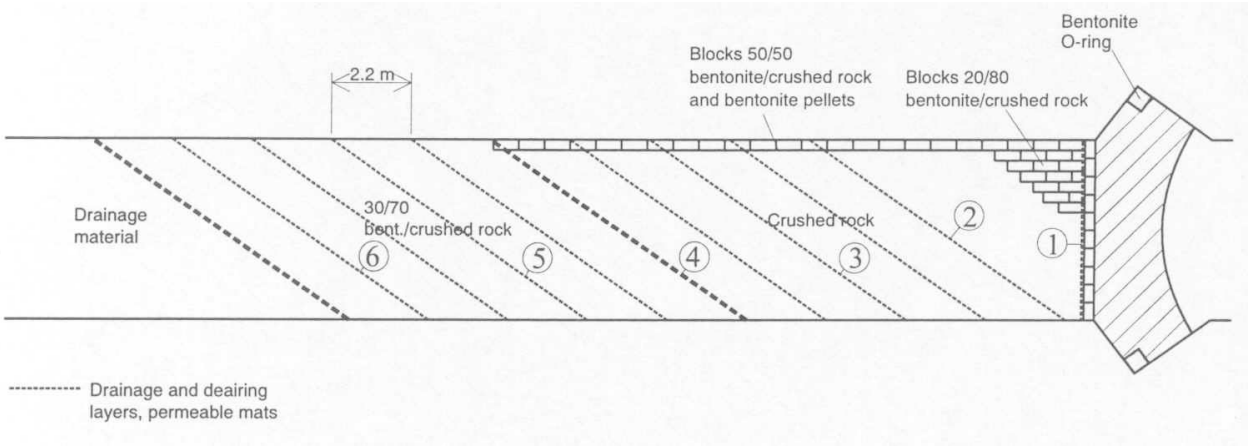

Figure 7-4. Location of filters 1-6 in Table 7-3.

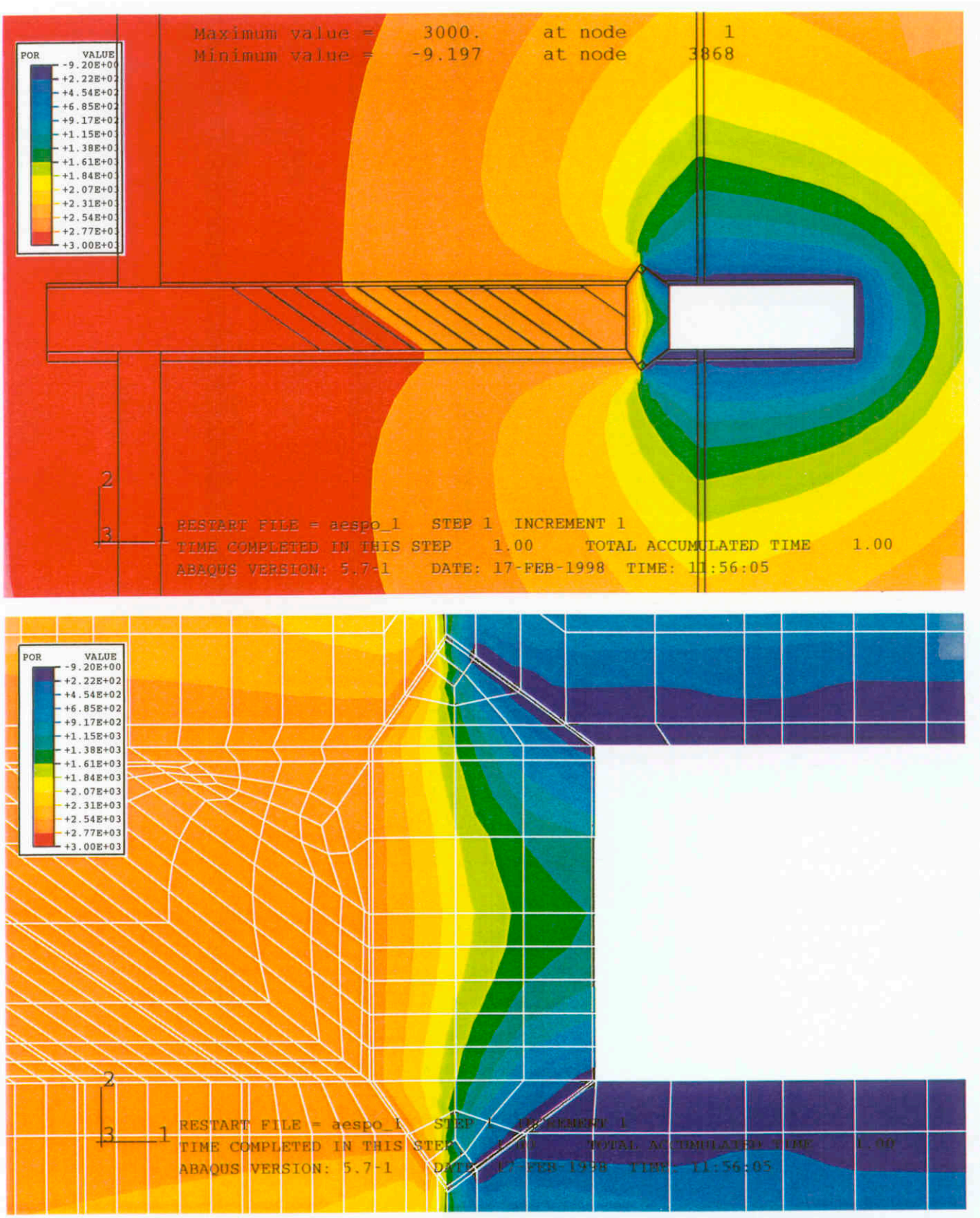

Figure 7-5. Calculation 1 (reference case after saturation). Pore water pressure (kPa) in the test area (upper) and at the plug

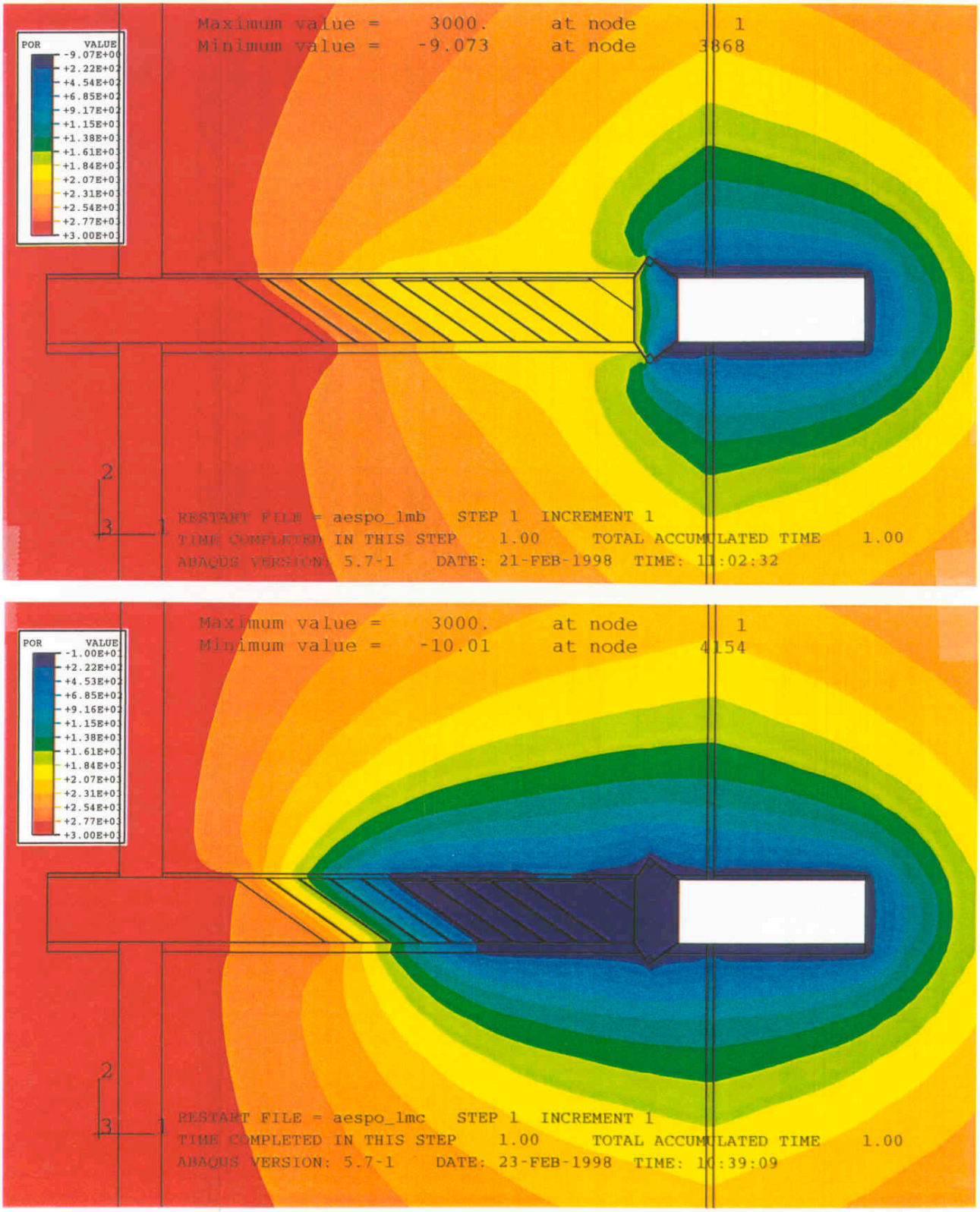

Figure 7-6. Two calculations showing the effect of a reduced sealing capacity of the plug on the pore water pressure distribution. Upper: $K=10^{-9}$ m/s of the bentonite o-ring (1mb). Lower: $K=10^{-1}$ m/s of the bentonite o-ring (1mc).

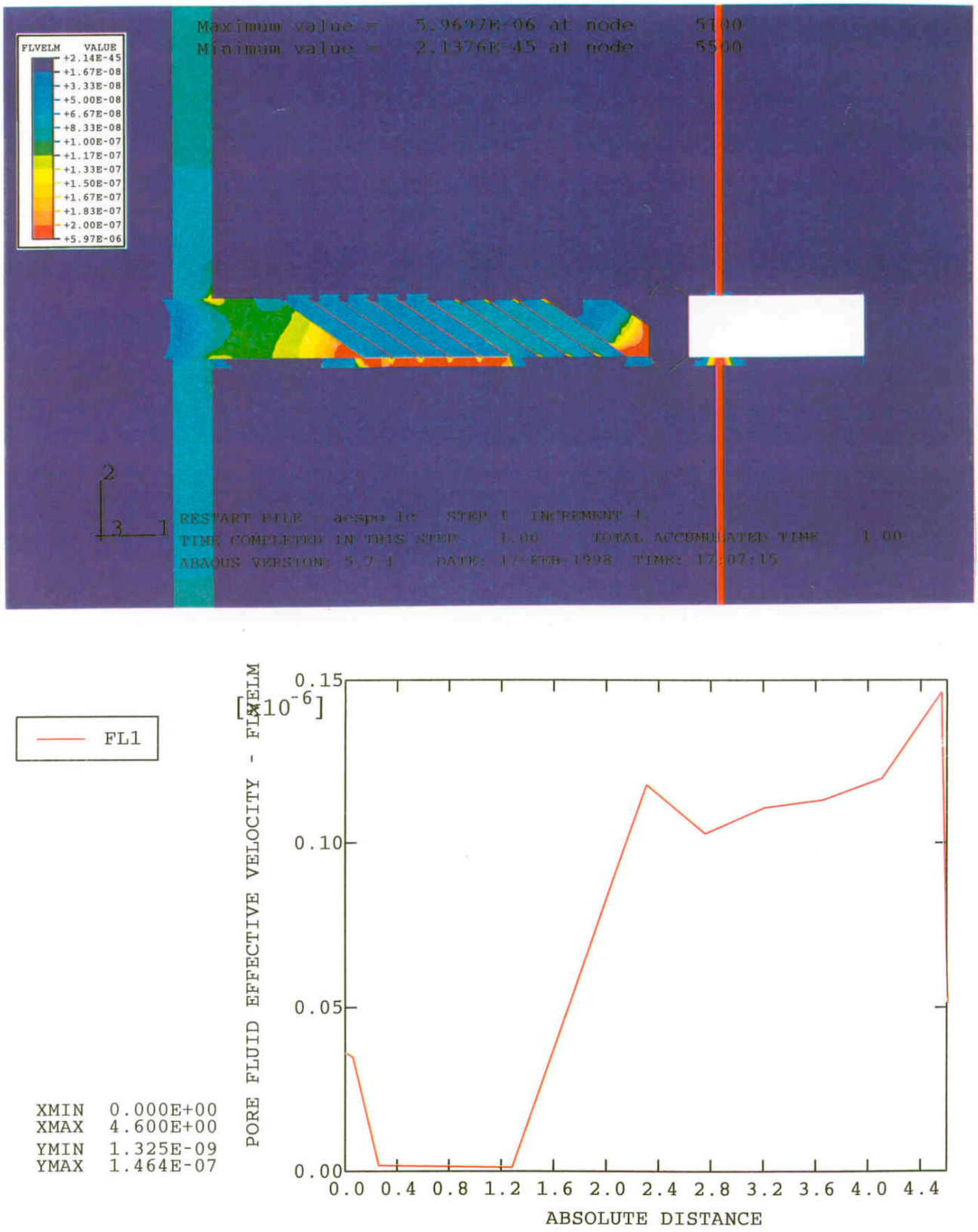

Figure 7-7. Calculation 1d1. Water flux ($m^3/s,m^2$) in the model (upper) and water flux into the filter on the plug wall as a function of the distance from the roof.

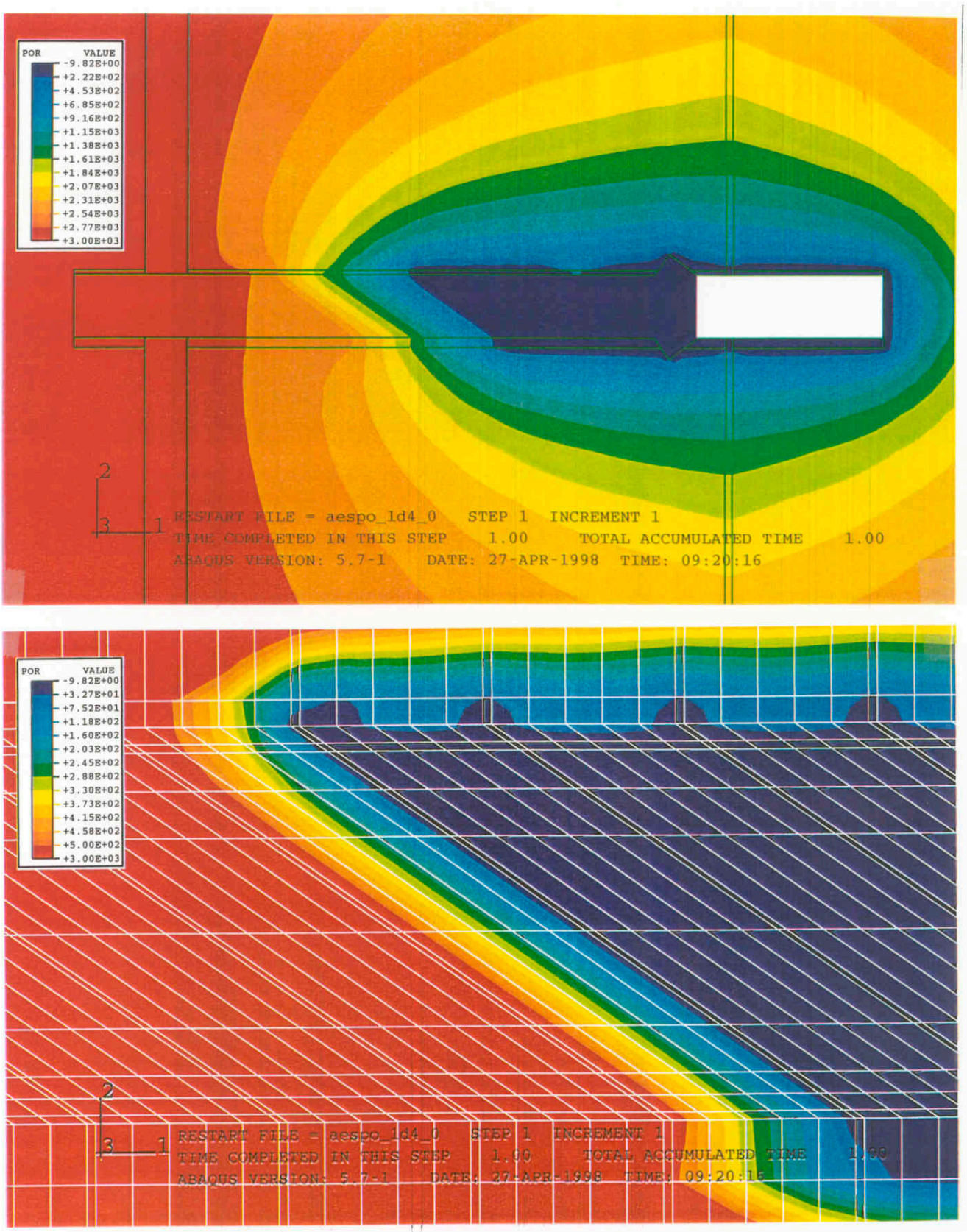

Figure 7-8. Calculation 1d4. Water pressure (kPa) in a large part of the model (upper) and around filter 4.

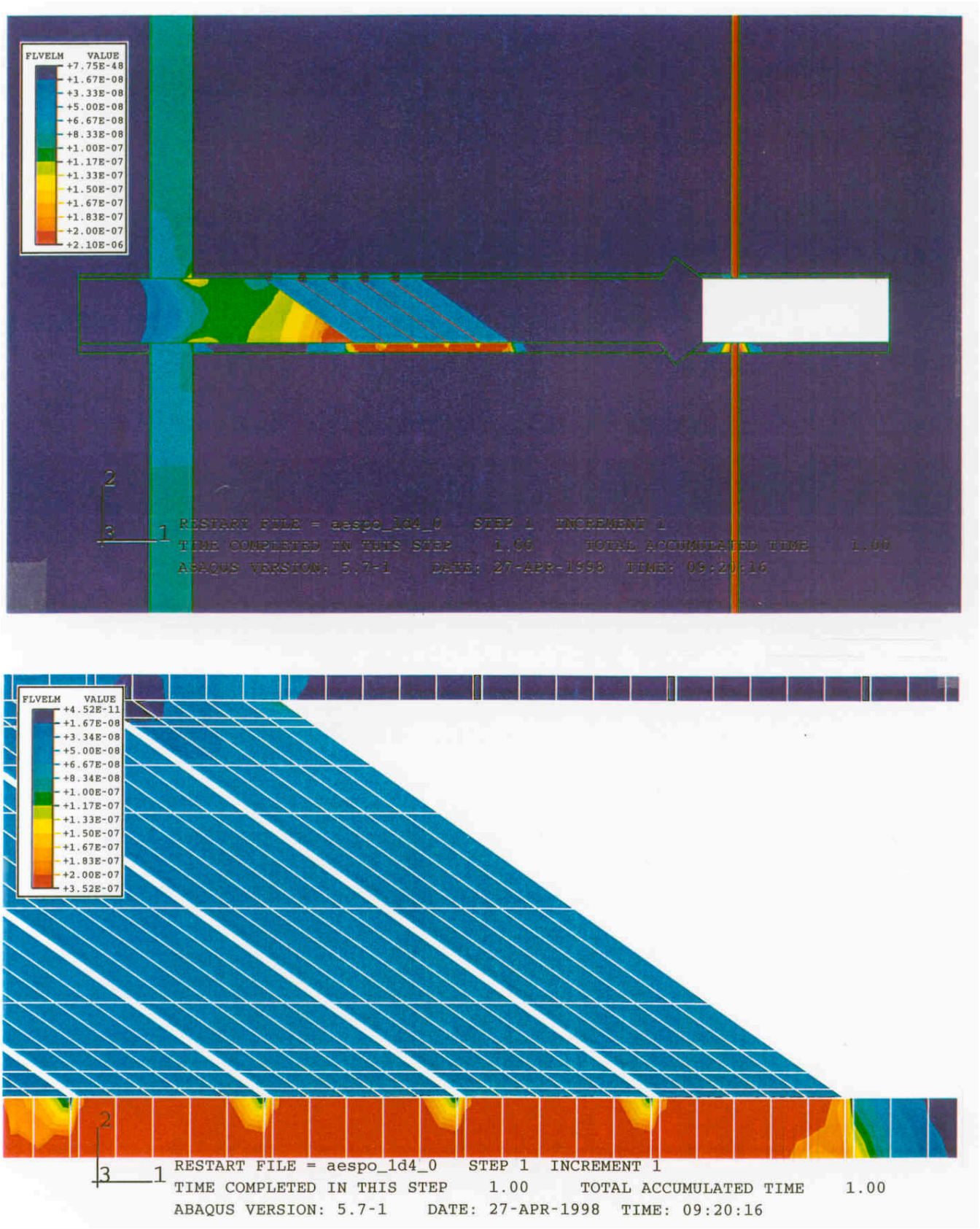

Figure 7-9. Calculation 1d4. Water flux ($m^3/s,m^2$) in a large part of the model (upper) and around filter 4.

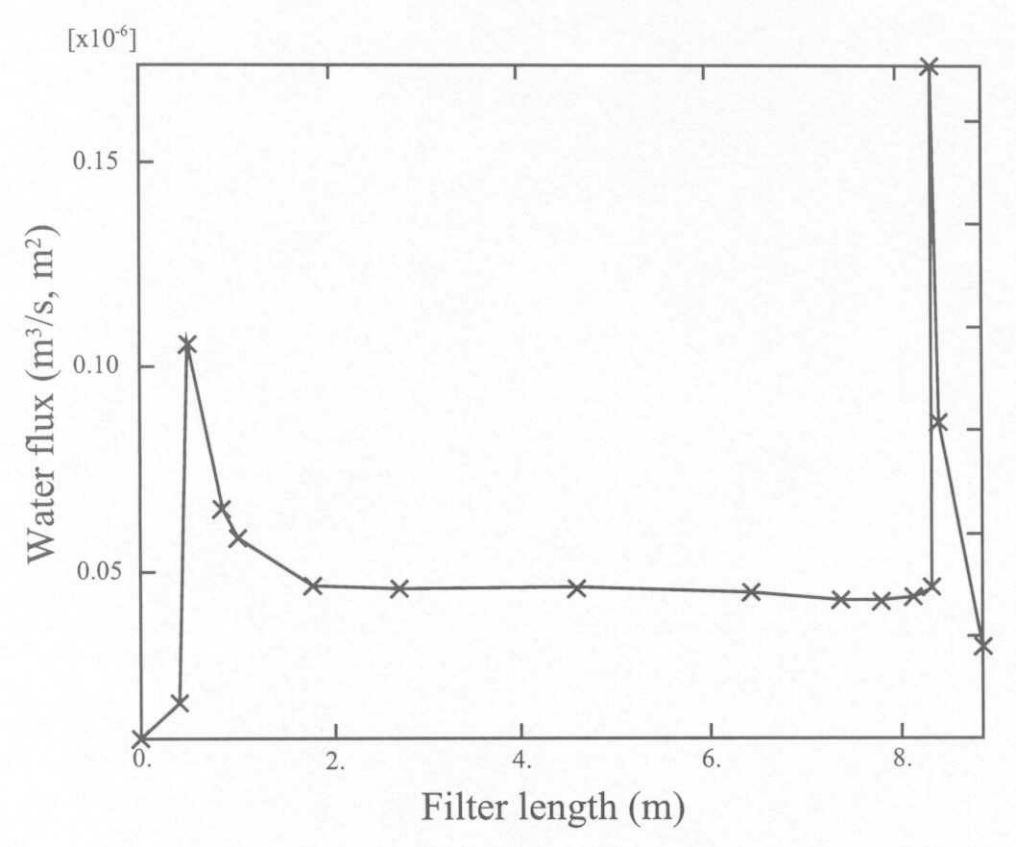

Figure 7-10. Calculation 1d4. Water flux ($m^3/s,m^2$) into filter 4 as a function of the length of the filter starting in the roof. 0.4 m of the filter is folded and attached to the rock in both the roof and the floor.

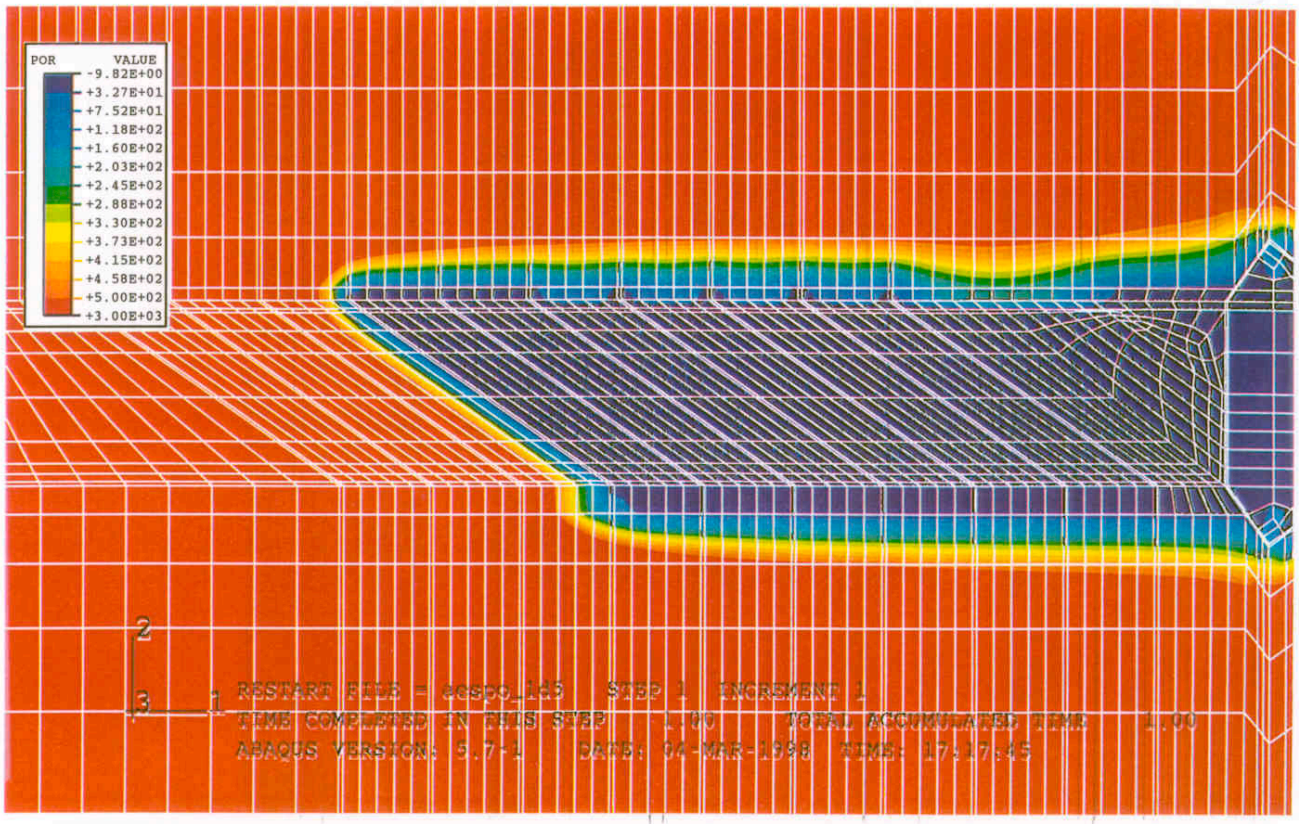

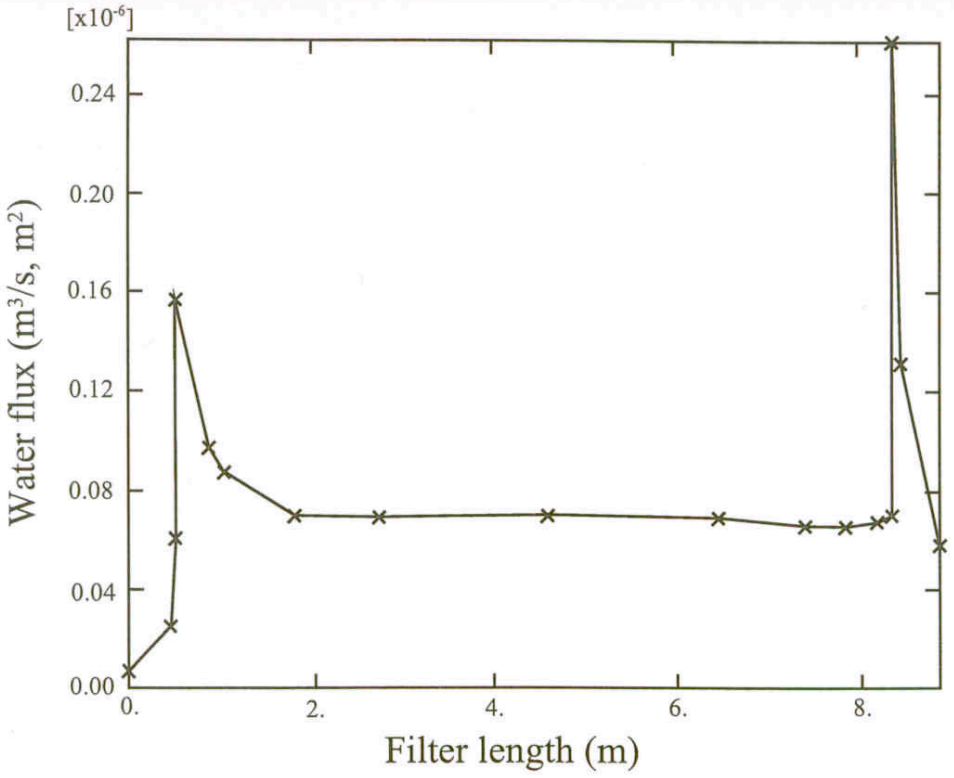

Figure 7-11. Calculation 1d5. Water pressure (kPa) distribution (upper) and water flux ($m^3/s,m^2$) into filter 5 as a function of the length of the filter starting in the roof. 0.4 m of the filter is folded and attached to the rock in both the roof and the floor.

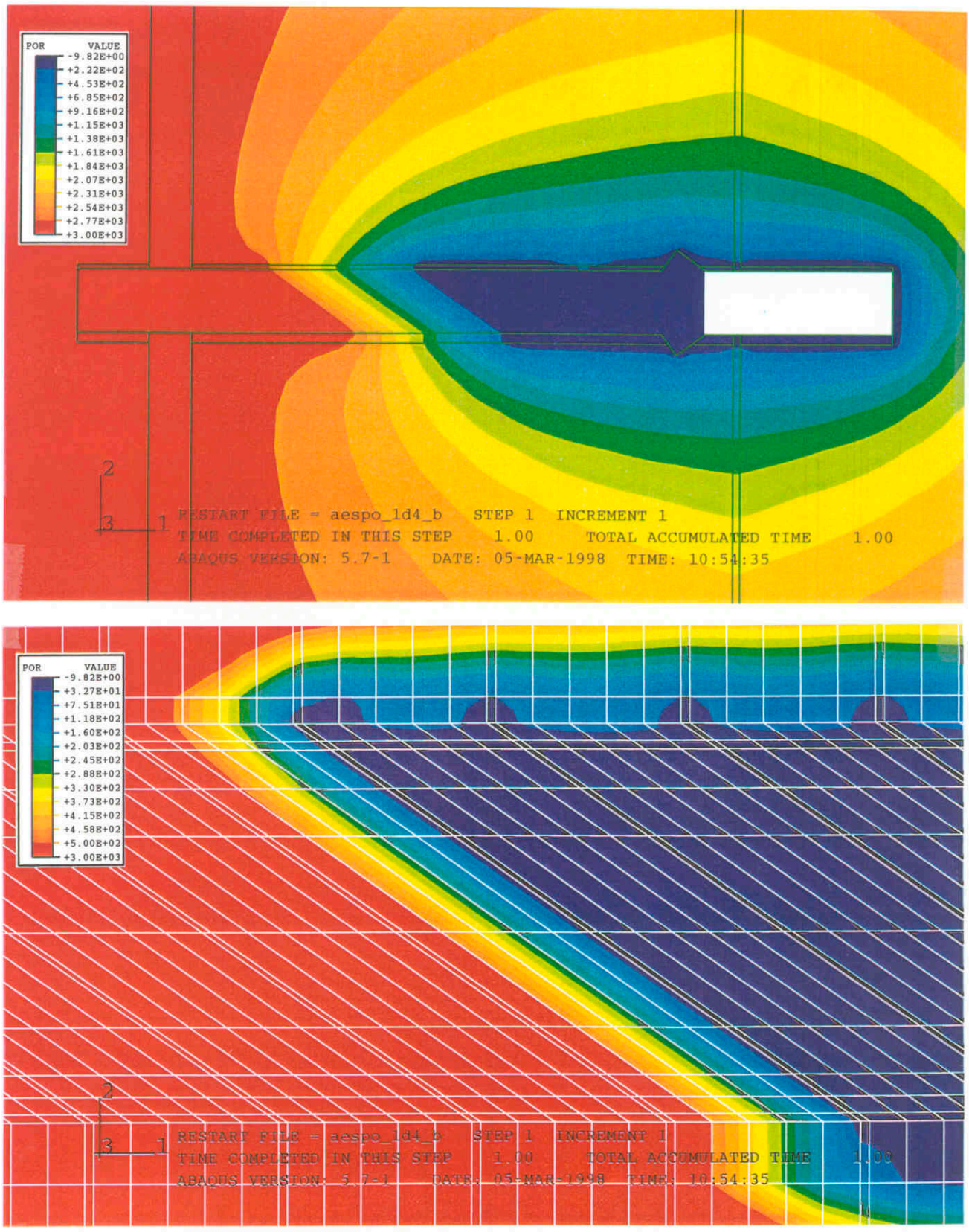

Figure 7-12. Calculation 1d4b (K(30/70) = 10^{-10} m/s). Water pressure (kPa) in a large part of the model (upper) and around filter 4.

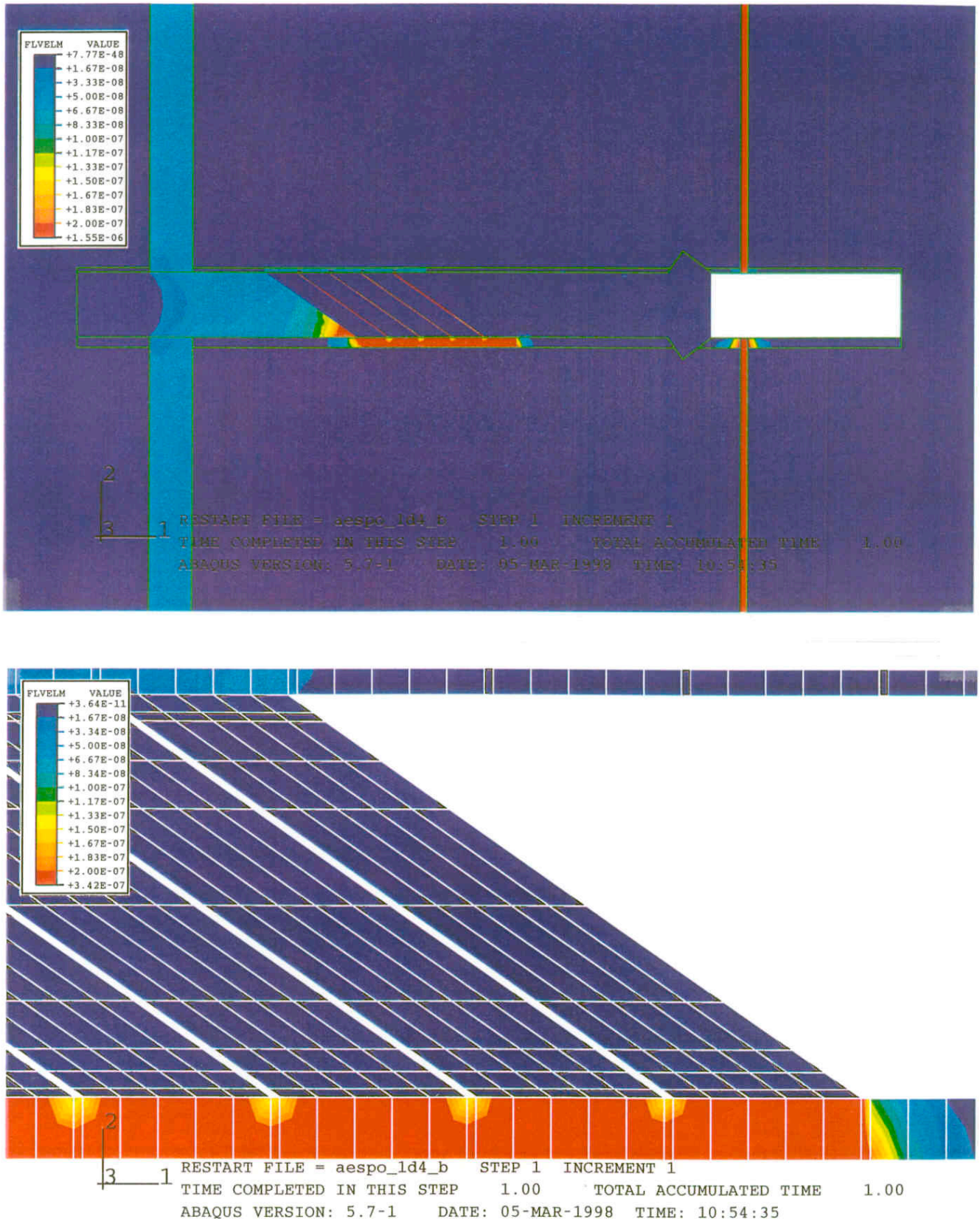

Figure 7-13. Calculation 1d4b (K(30/70) = 10^{-10} m/s). Water flux ($m^3/s,m^2$) in a large part of the model (upper) and around filter 4.

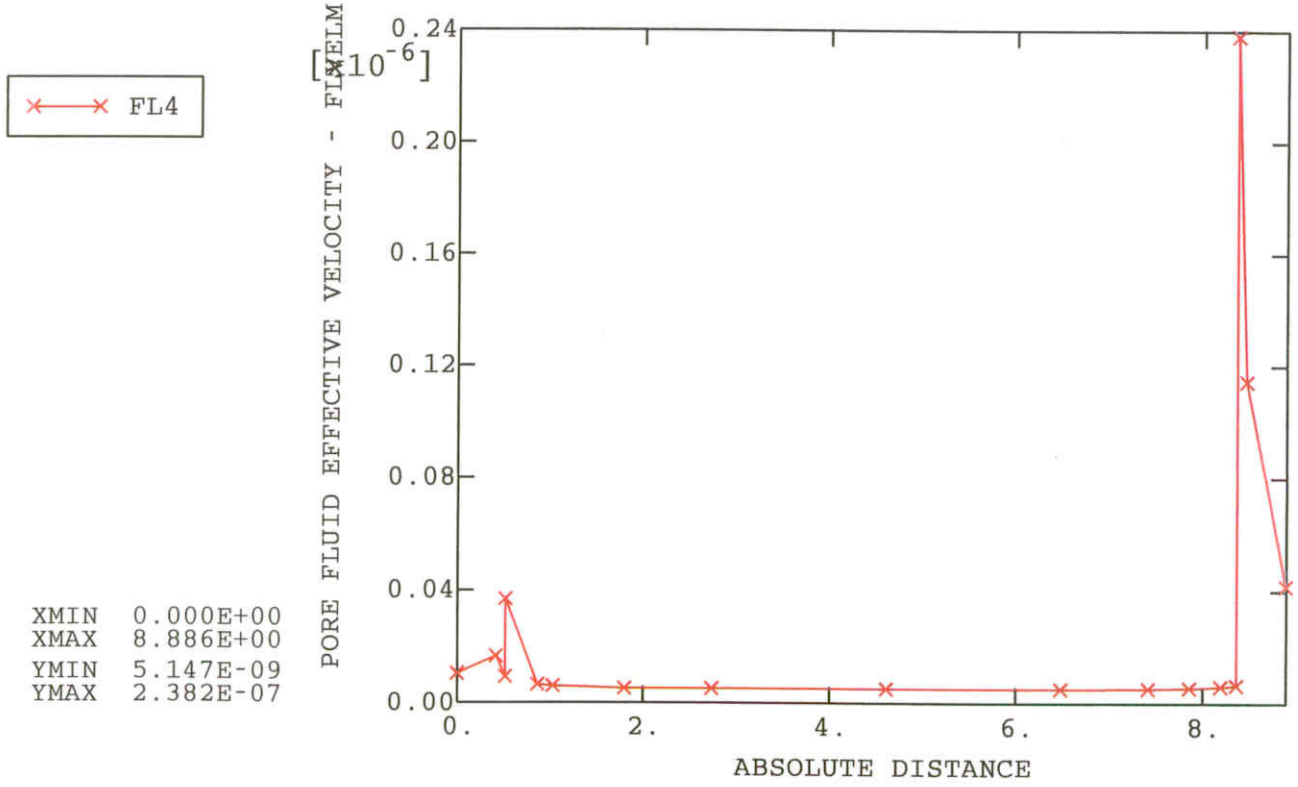

Figure 7-14. Calculation 1d4b (K(30/70) = 10^{-10} m/s). Water flux ($m^3/s,m^2$) into filter 4 as a function of the length of the filter starting in the roof. 0.4 m of the filter is folded and attached to the rock in both the roof and the floor.

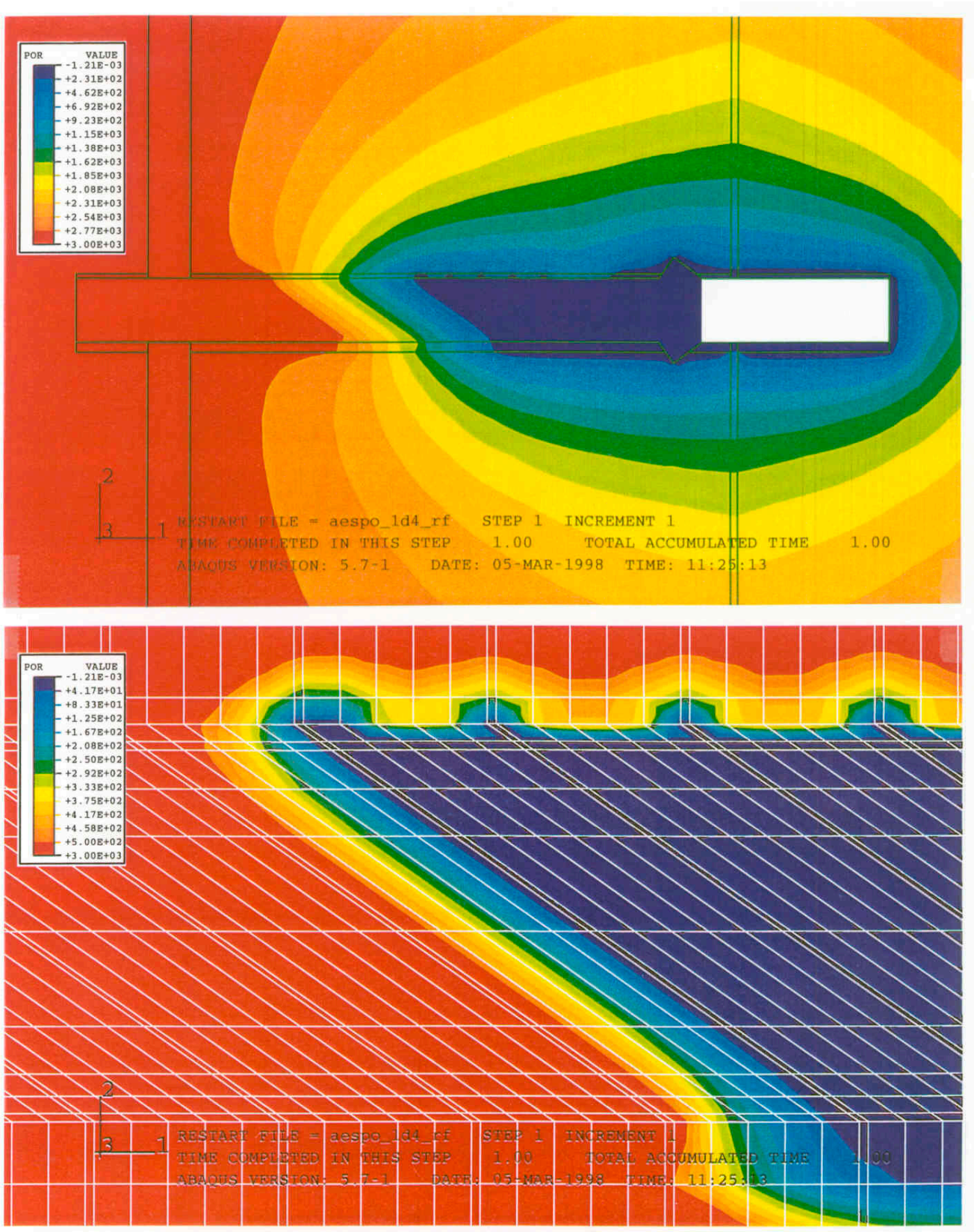

Figure 7-15. Calculation 1d4rf (K(roof) = 10^{-10} m/s; K(floor) = 10^{-9} m/s). Water pressure (kPa) in a large part of the model (upper) and around filter 4.

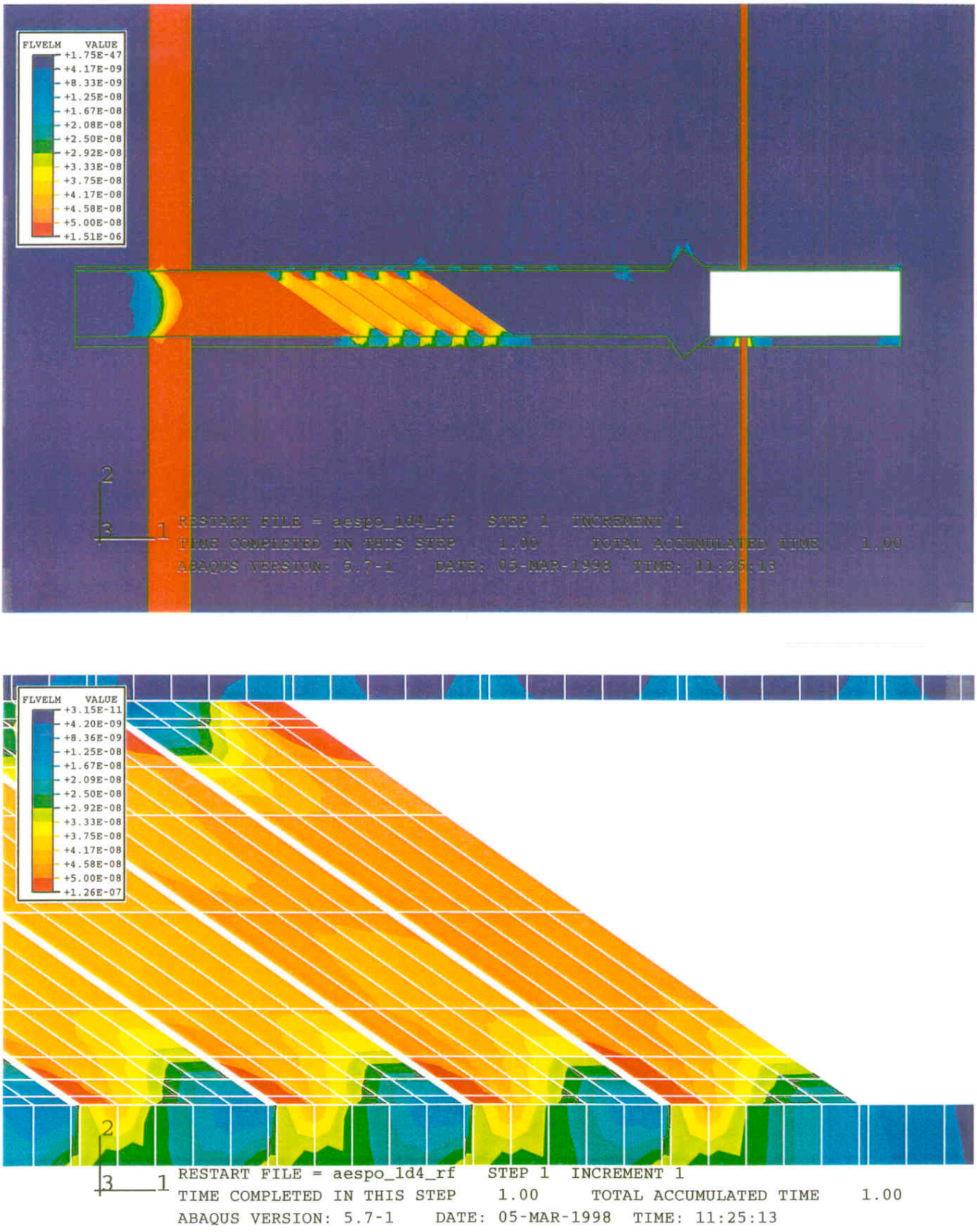

Figure 7-16. Calculation 1d4rf (K(roof) = 10^{-10} m/s; K(floor) = 10^{-9} m/s). Water flux ($m^3/s,m^2$) in a large part of the model (upper) and around filter 4.

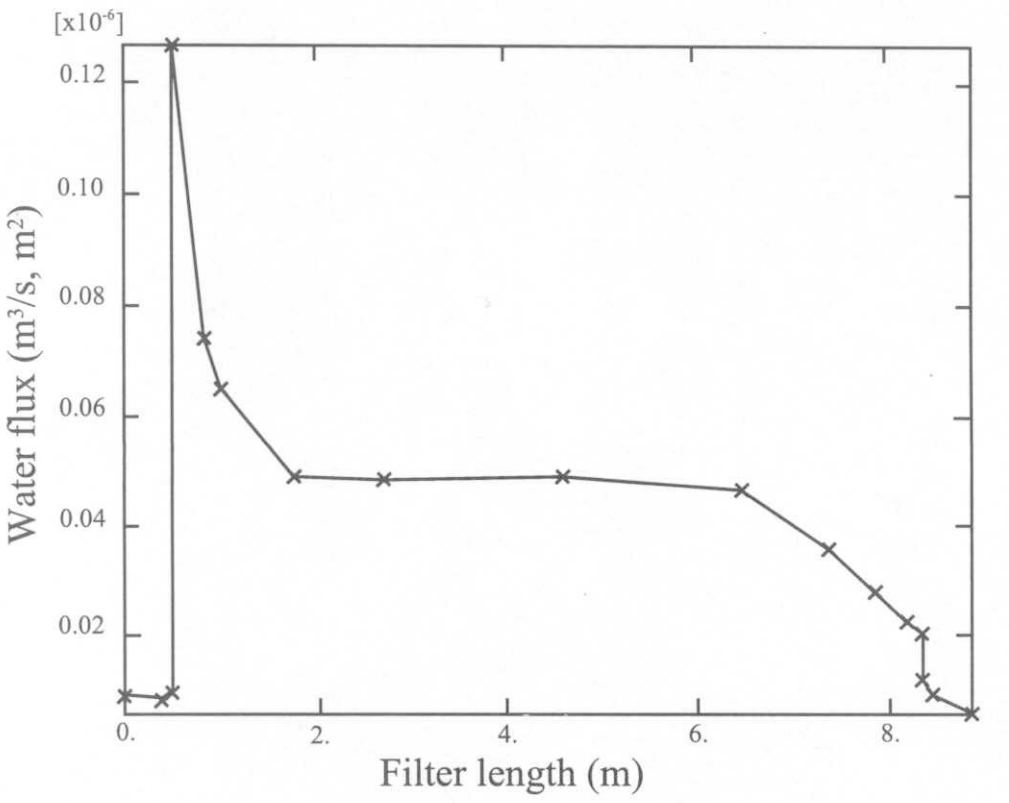

Figure 7-17. Calculation 1d4rf (K(roof) = 10^{-10} m/s; K(floor) = 10^{-9} m/s). Water flux ($m^3/s,m^2$) into filter 4 as a function of the length of the filter starting in the roof. 0.4 m of the filter is folded and attached to the rock in both the roof and the floor.

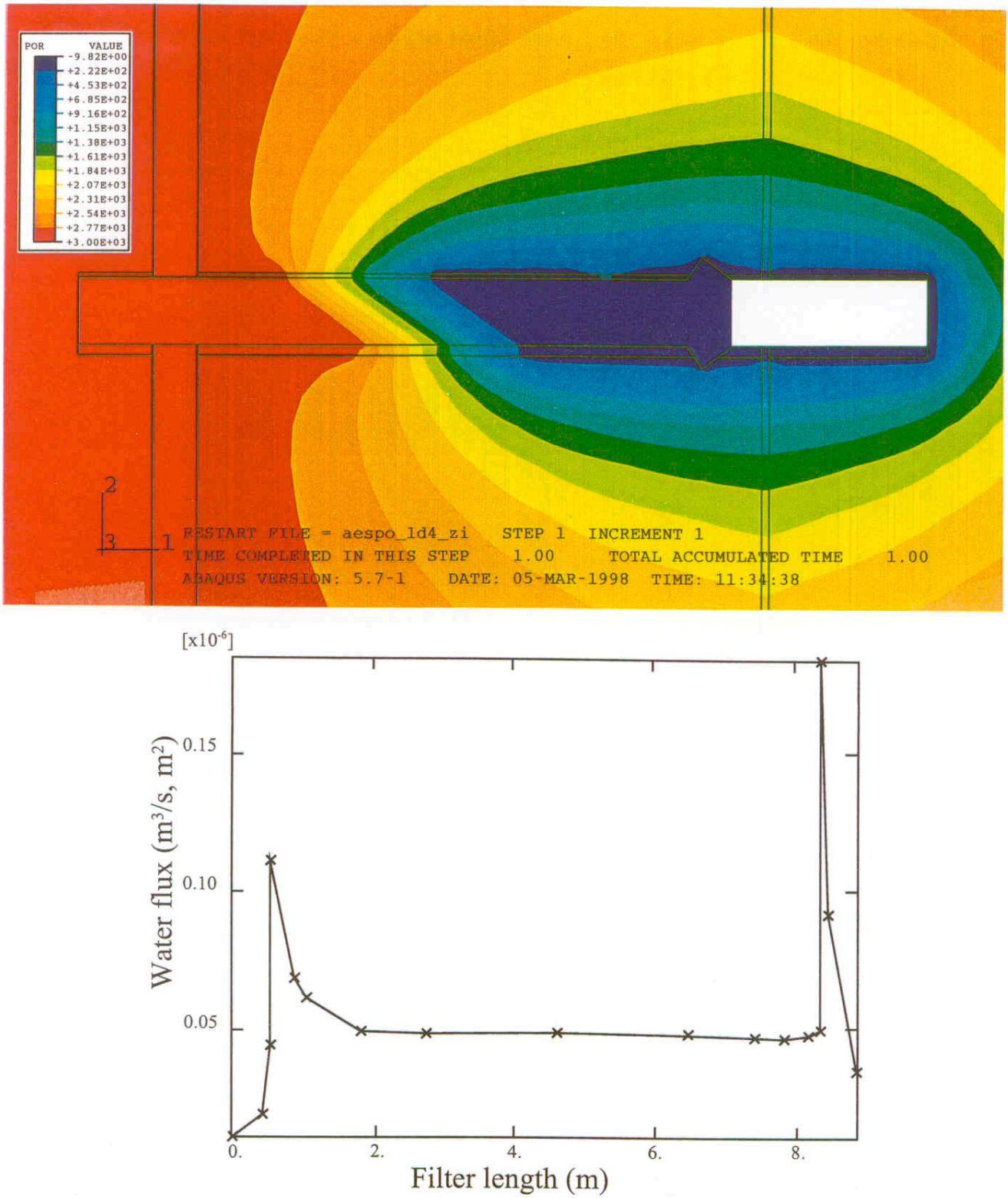

Figure 7-18. Calculation 1d4zi (K(fract. zone) = $4 \cdot 10^{-7}$ m/s). Water pressure (kPa) in a large part of the model (upper) and water flux ($m^3/s,m^2$) into filter 4 as a function of the length of the filter starting in the roof. 0.4 m of the filter is folded and attached to the rock in both the roof and the floor.

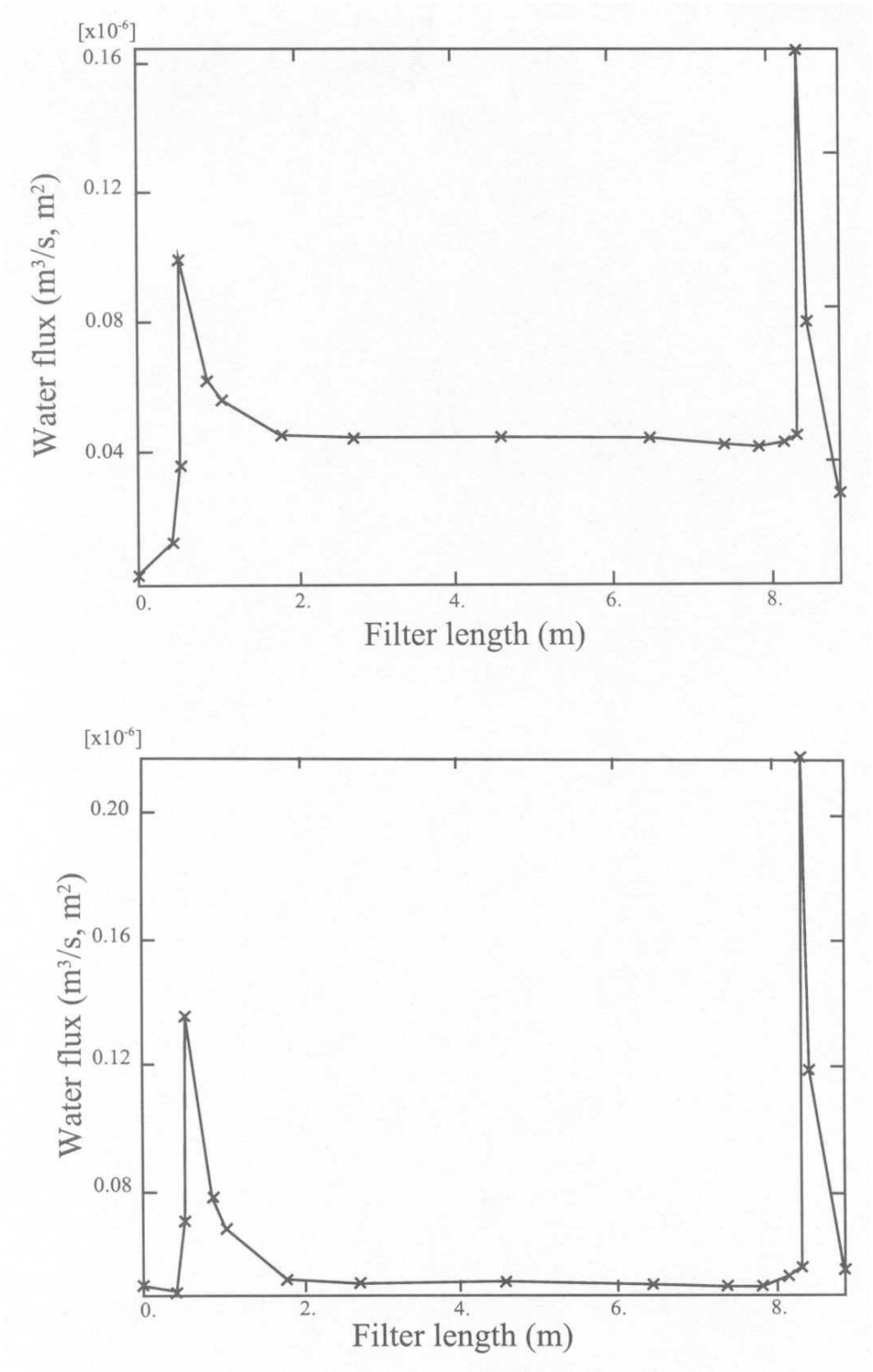

Figure 7-19. Calculation 1d4r01 (upper) and 1d4r02 (K(rock) = 10^{-11} m/s respectively $3 \cdot 10^{-10}$ m/s). Water flux ($m^3/s,m^2$) into filter 4 as a function of the length of the filter starting in the roof. 0.4 m of the filter is folded and attached to the rock in both the roof and the floor.

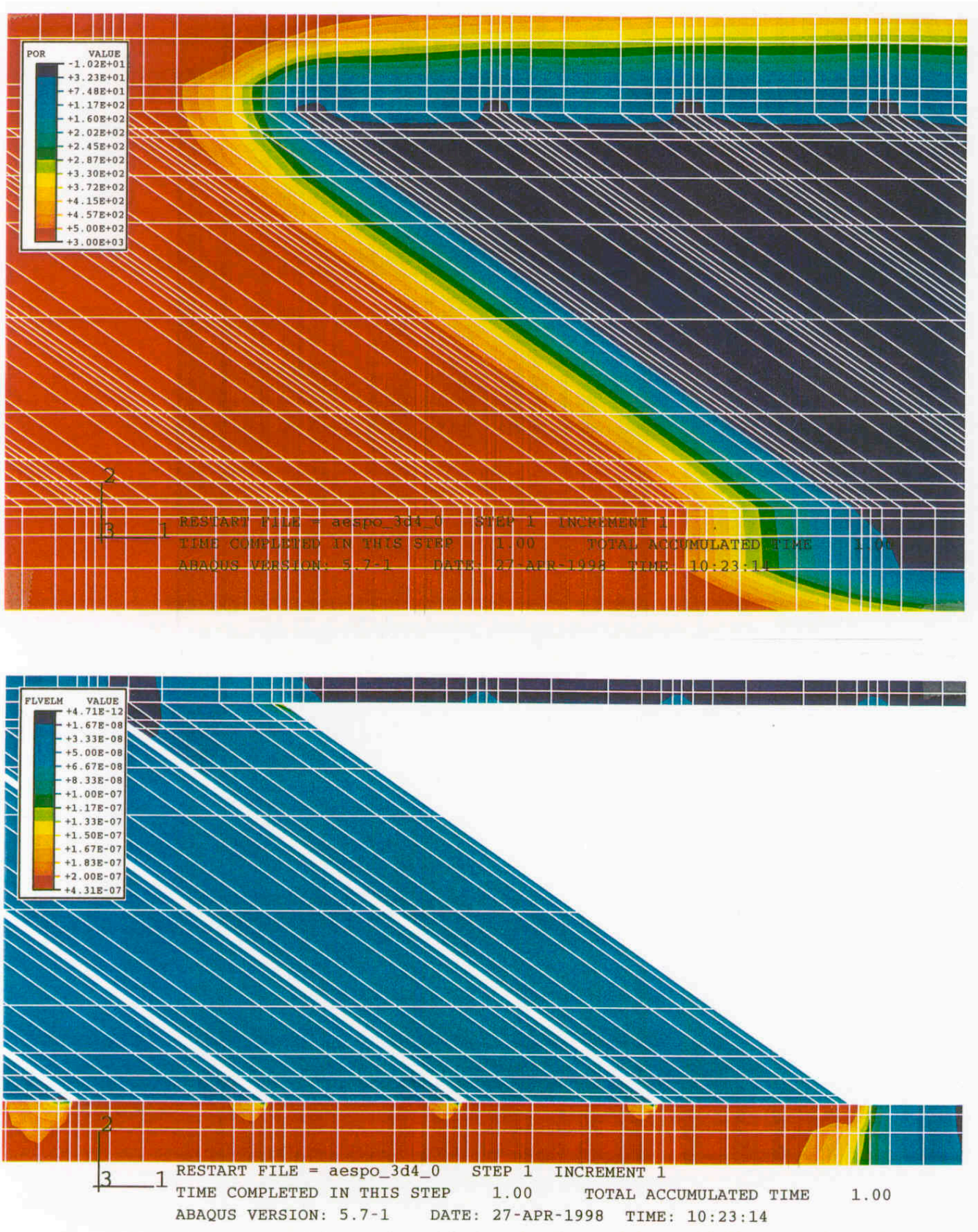

Figure 7-20. Calculation 3d40 (reference case with refined mesh). Water pressure (kPa) (upper) and water flux ($m^3/s,m^2$) around filter 4.

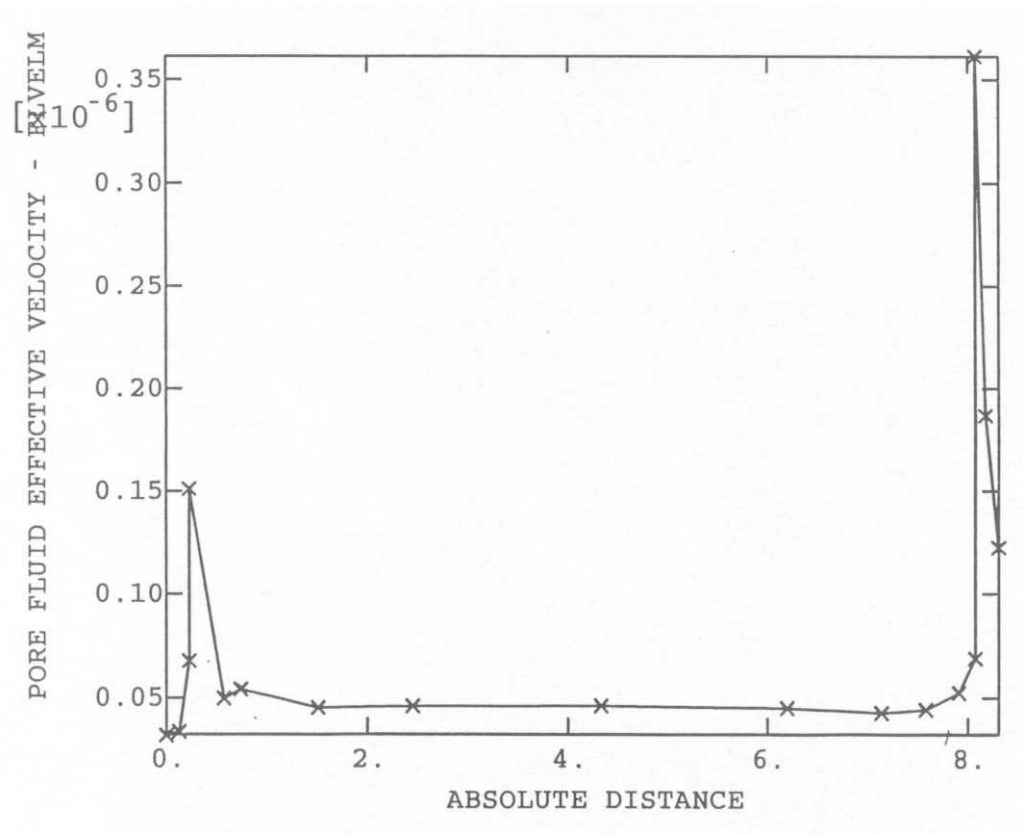

Figure 7-21. Calculation 3d40 (reference case with refined mesh). Water flux ($m^3/s,m^2$) into filter 4 as a function of the length of the filter starting in the roof. 0.4 m of the filter is folded and attached to the rock in both the roof and the floor.

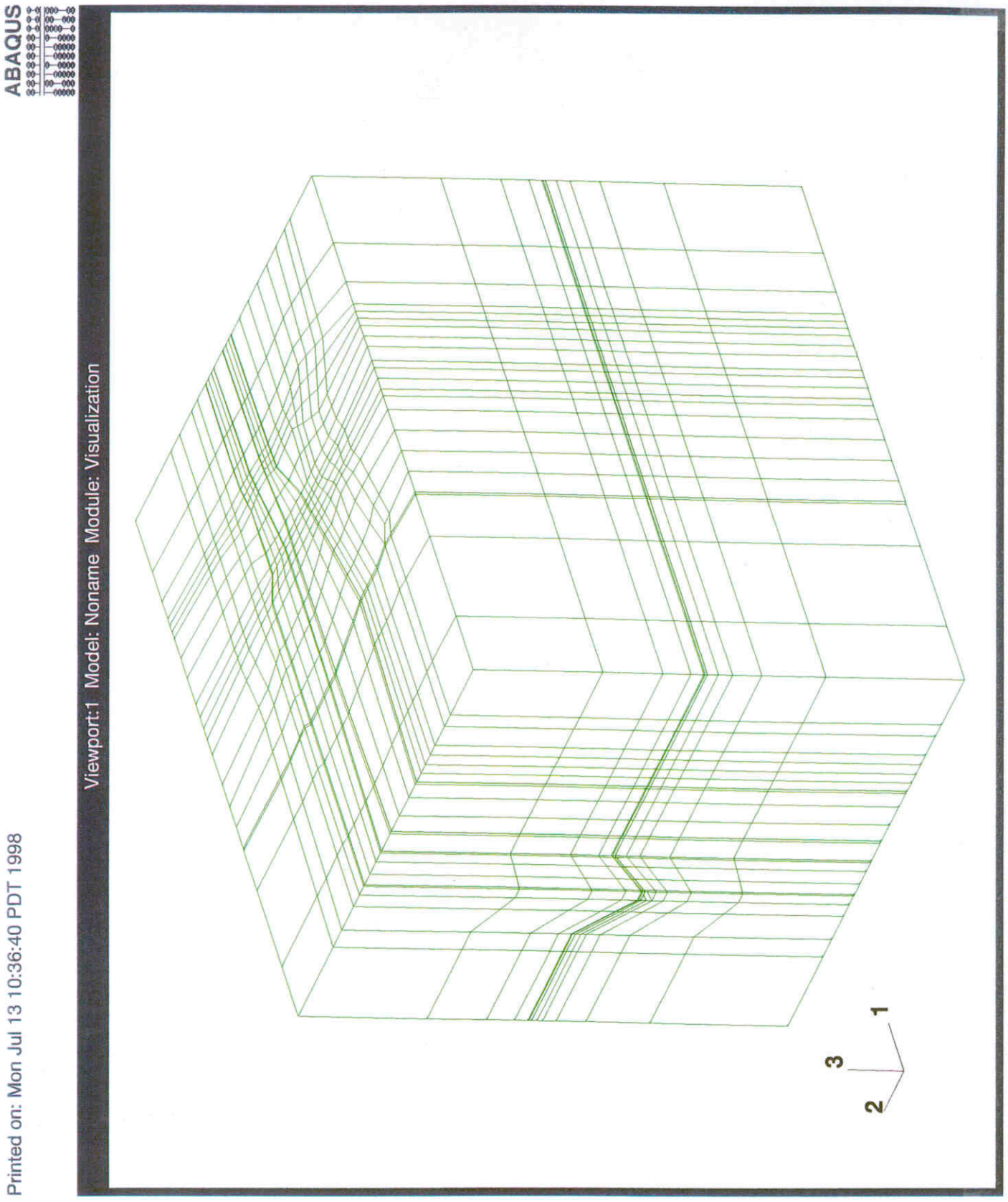

Figure 8-1. Element mesh for the large scale 3D model.

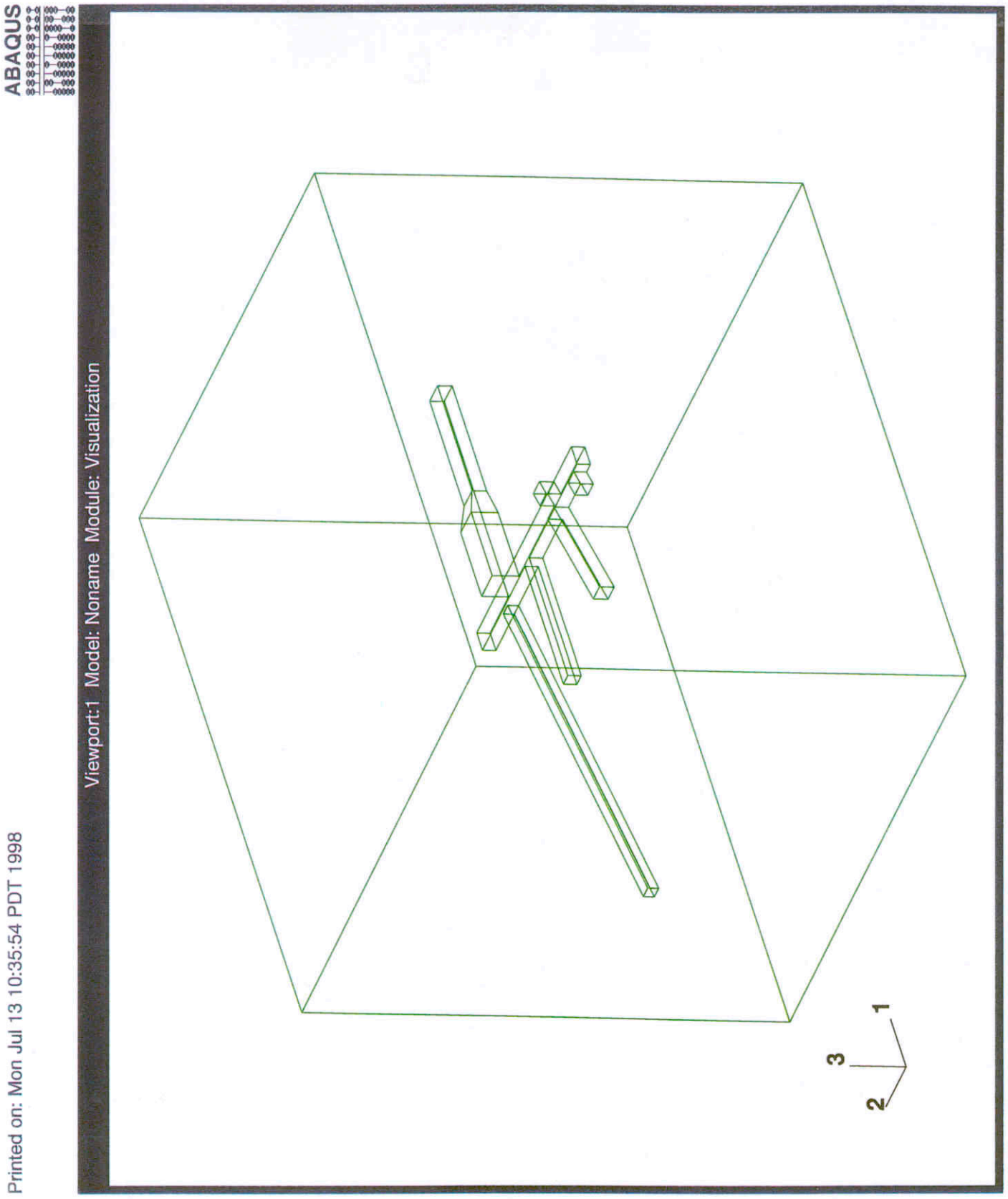

Figure 8-2. Excavations in the large scale 3D model.

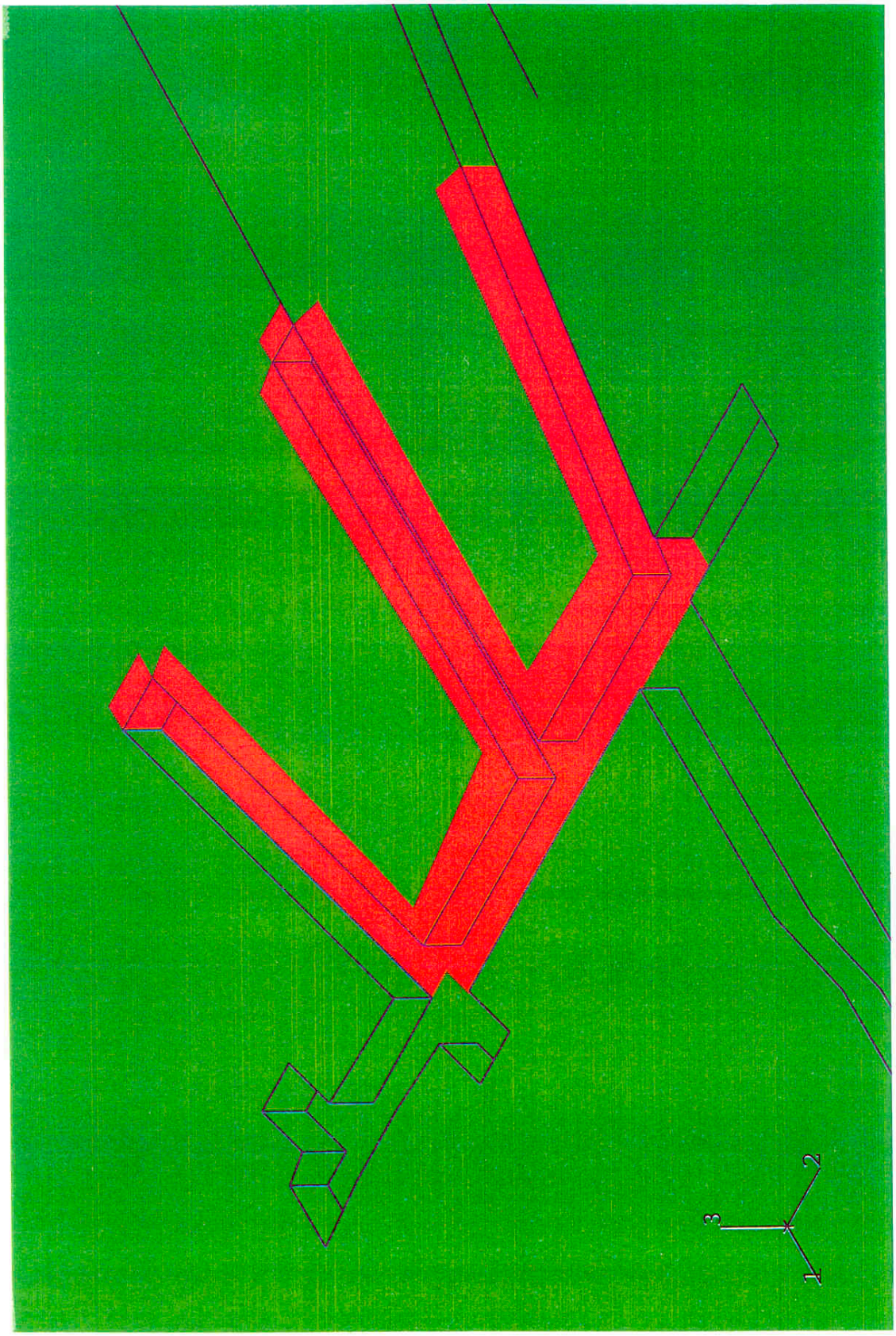

Figure 8-3. Skin zone with decreased hydraulic conductivity (red areas).

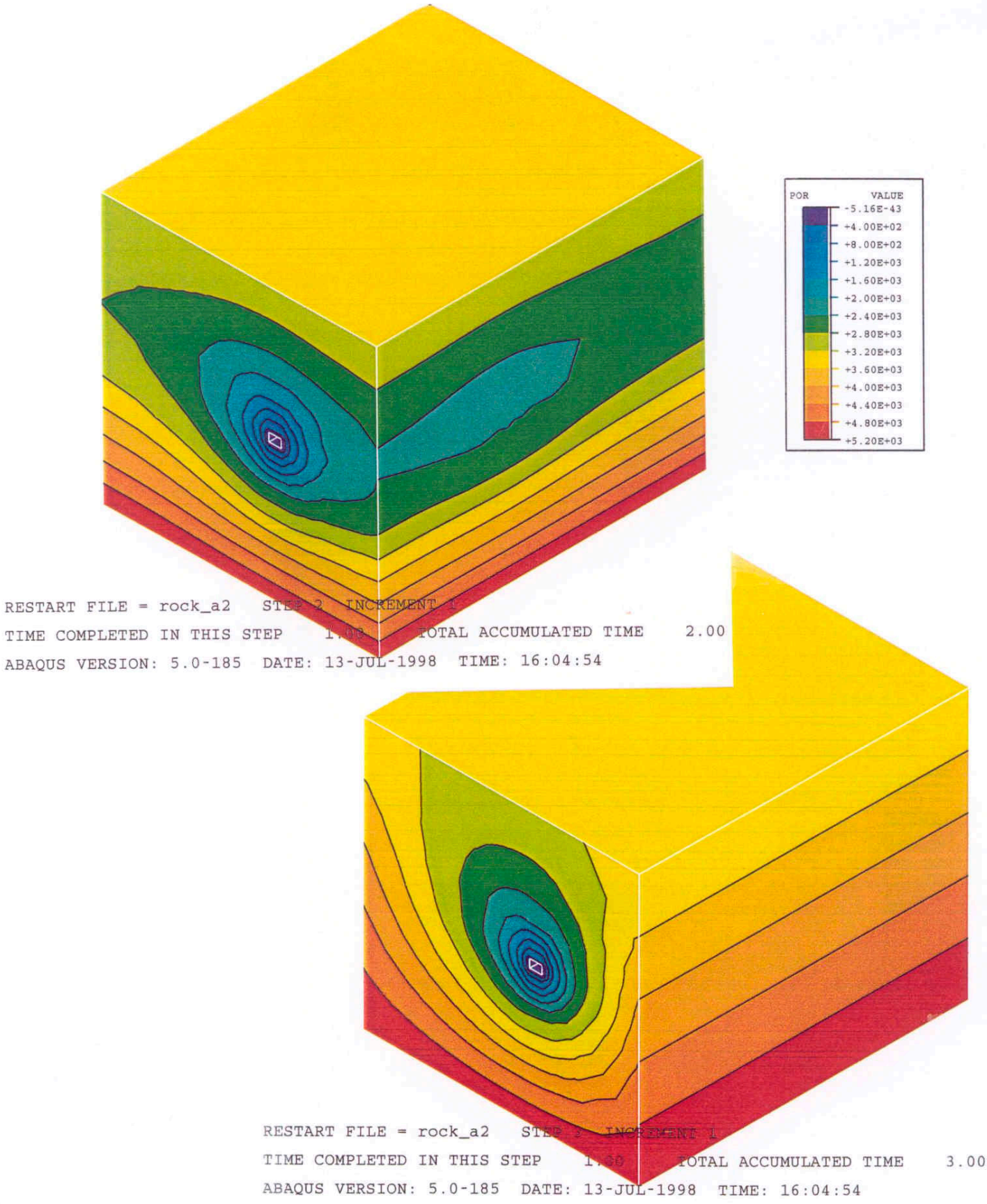

Figure 8-4. Water pressure (kPa) at the outer boundaries in calculations a22 (upper) and a23.

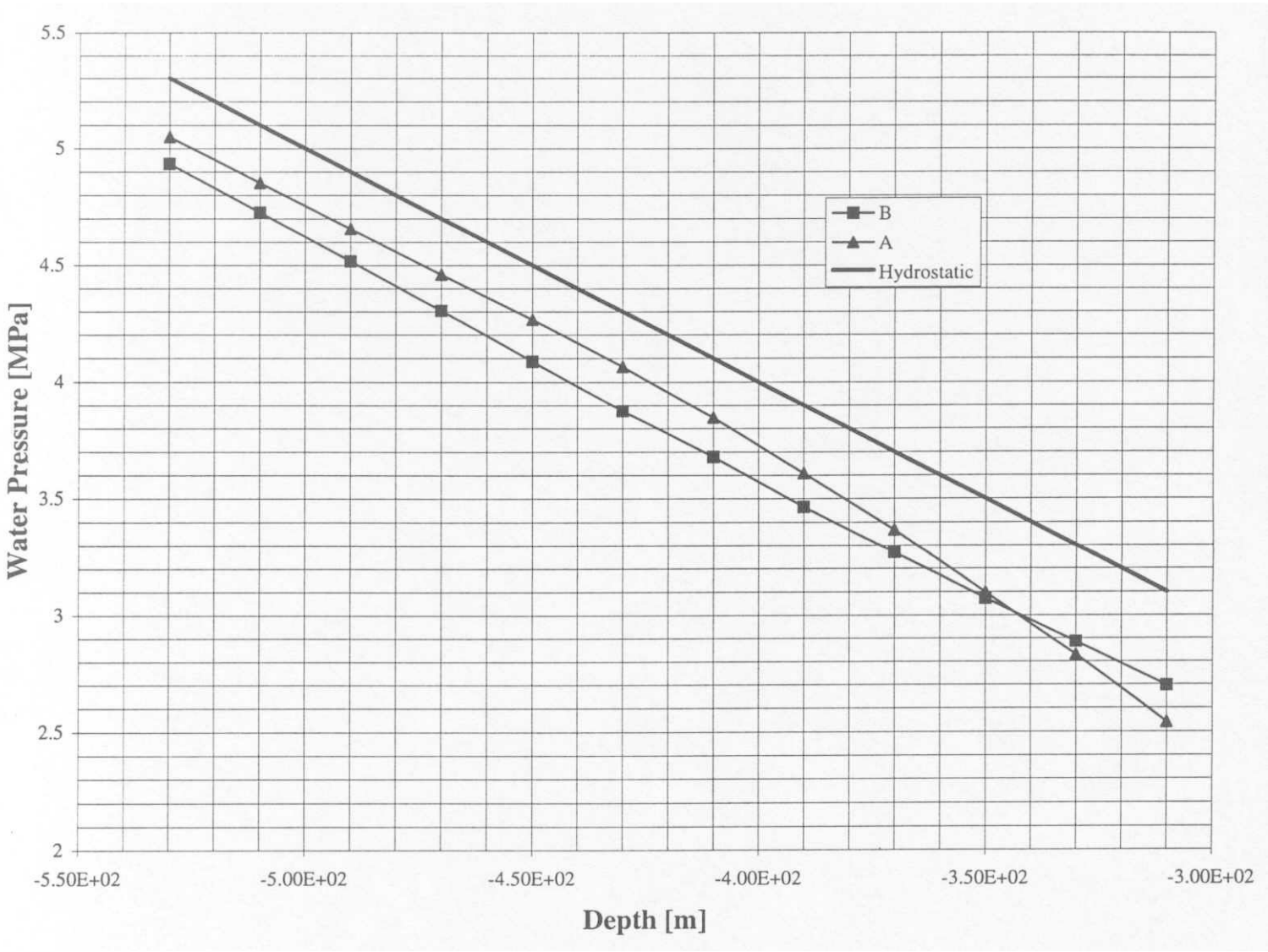

Figure 8-5. Water pressure as a function of depth in a regional scale /8-2/ at two vertical lines in the centre of the two planes defining boundary 3 (see Table 8-4)

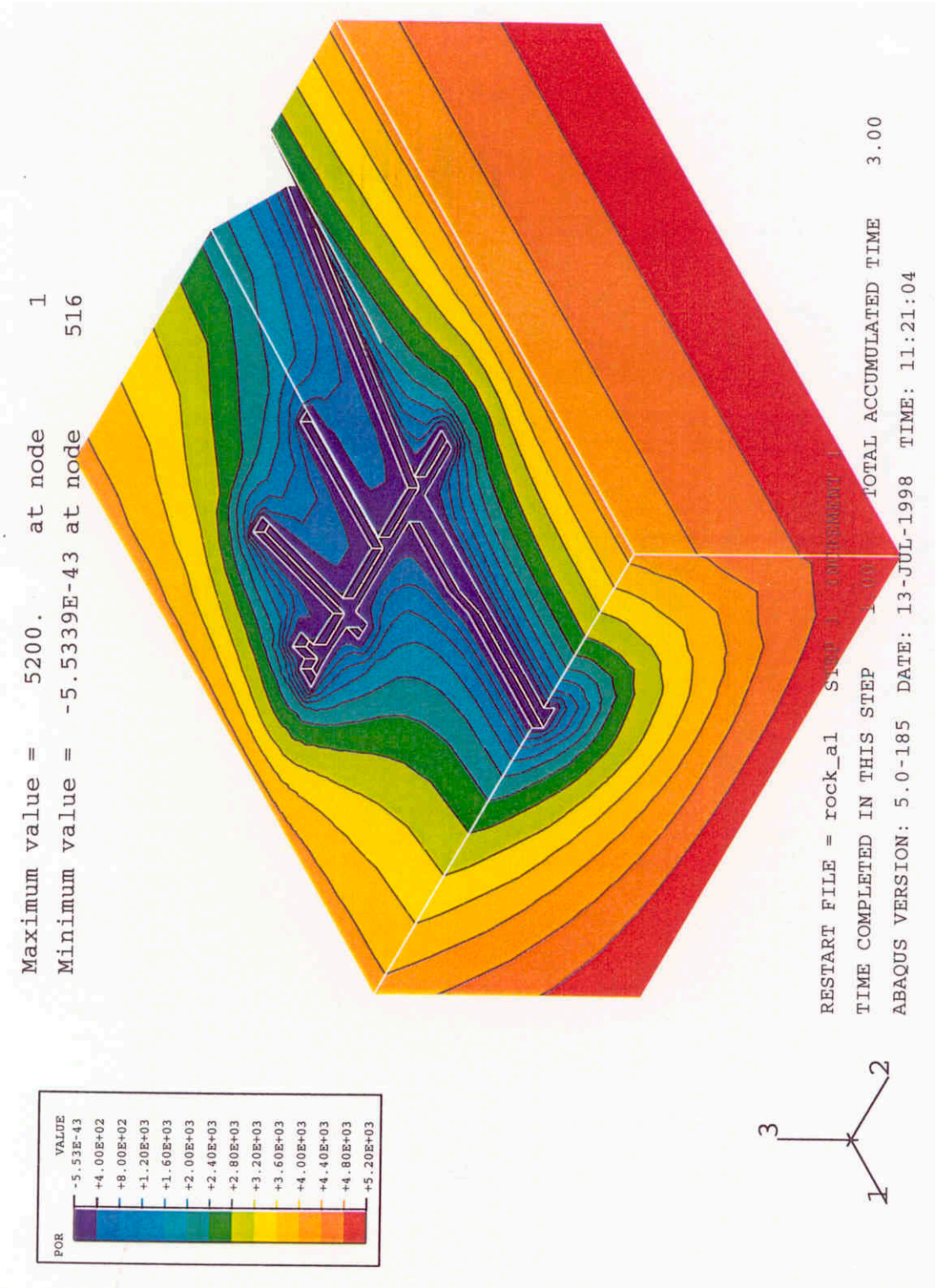

Figure 8-6. Water pressure distribution (kPa) in calculation a13 with no skin factor (S_f = 1)

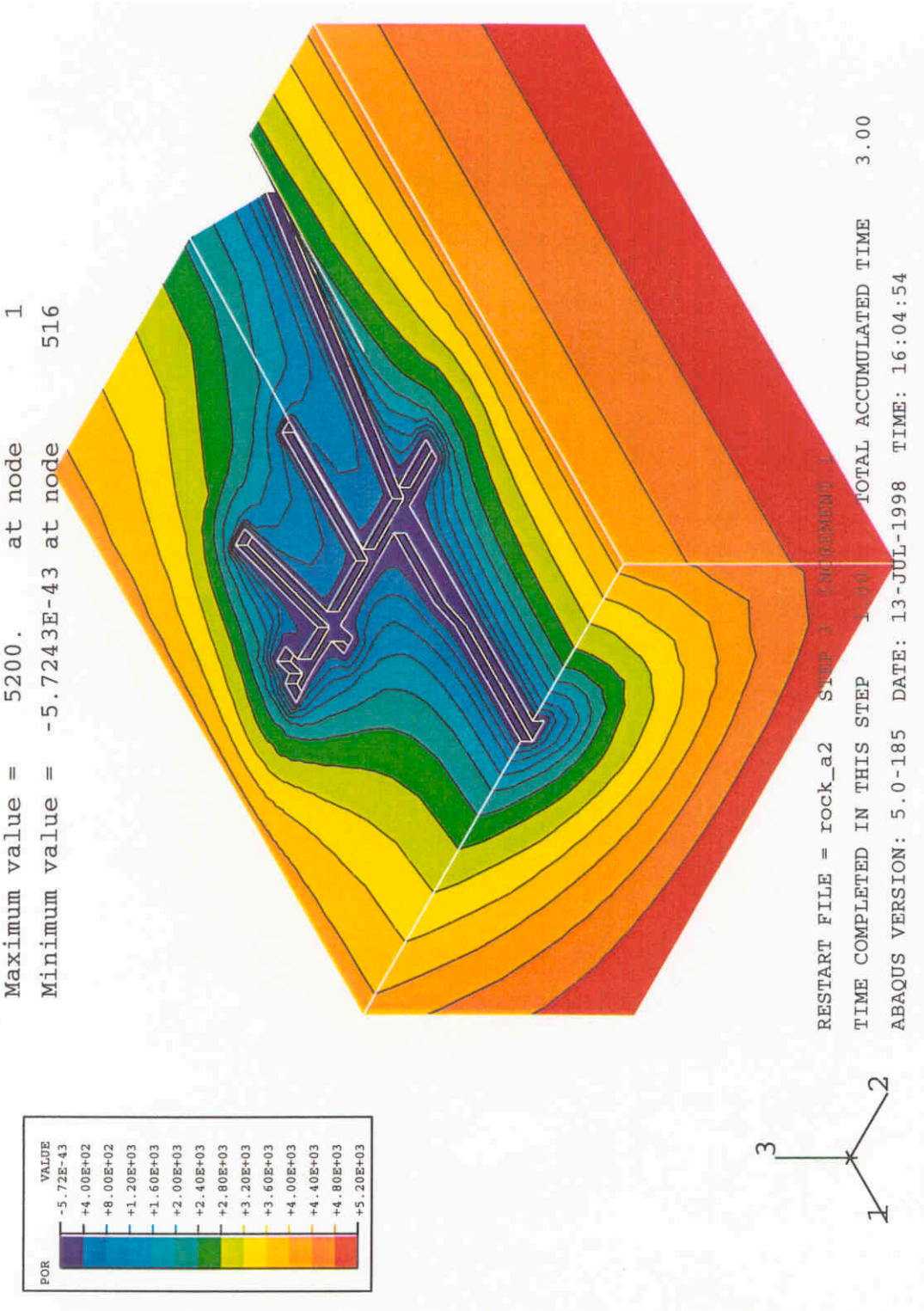

Figure 8-7. Water pressure distribution (kPa) in calculation a13 with skin factor (S_f = 0.25)

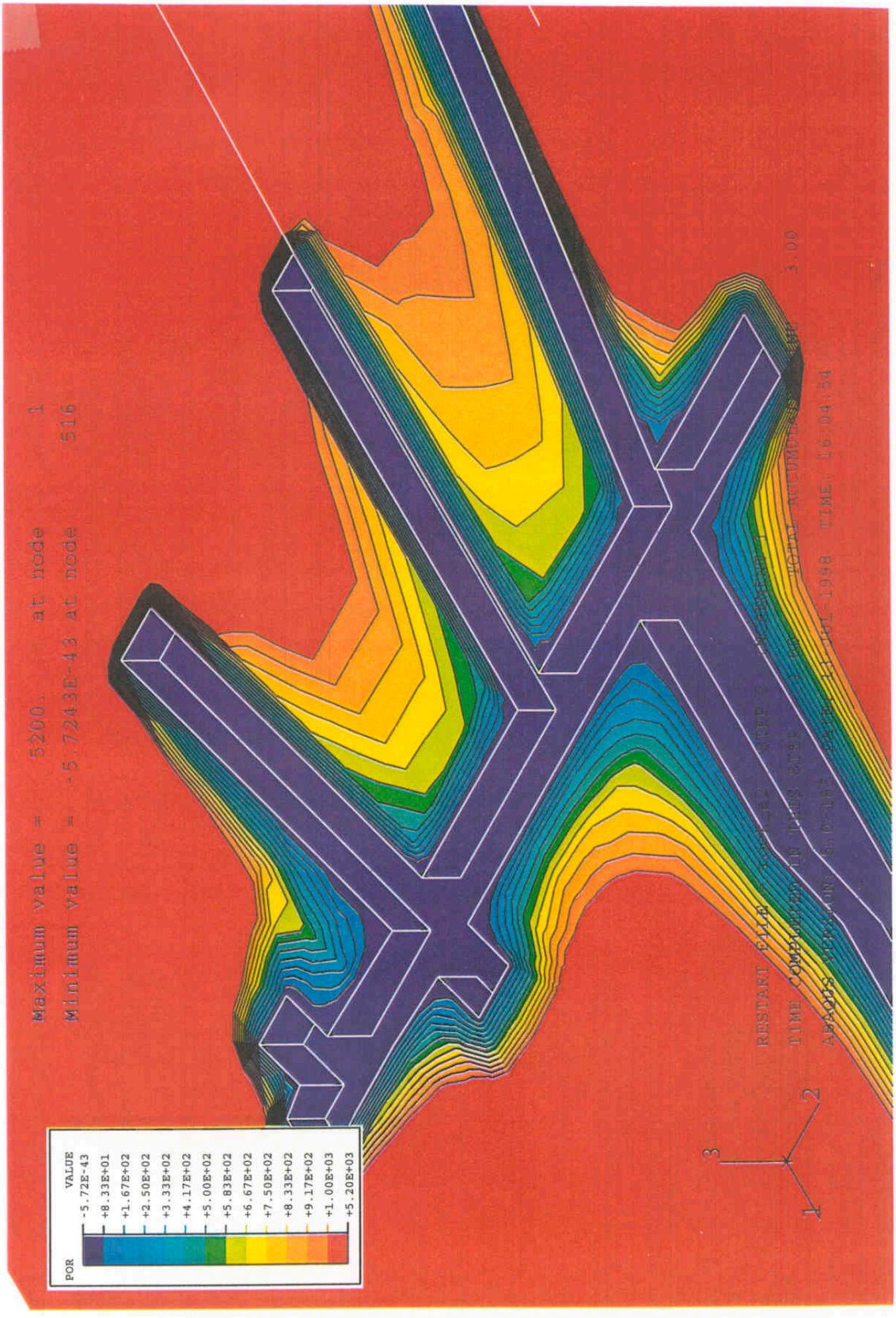

Figure 8-8. A detail of Fig 8-7. Water pressure distribution (kPa) in calculation a23 with skin factor (S_f = 0.25)